Kinematic modelisation and parametric study of mechanosynthesis of hydroxyfluorapatite

Hanen Hajji, Mohieddine Abdellaoui, Lionel Maurizi, Samia Nasr, Nadine Millot, Ezzedine Ben Salem

Kinematic modelisation and parametric study of mechanosynthesis of hydroxyfluorapatite

Hanen Hajji[a,c*], Mohieddine Abdellaoui[b,*], Lionel Maurizi[c], Samia Nasr[d], Nadine Millot[c,*] and Ezzedine Ben Salem[a]

[a] I.P.E.I. of Monastir, Unit of Materials and Organic Synthesis, University of Monastir, Tunisia

[b] Institut National de Recherche et d'Analyse Physico-Chimique, Pôle Technologique de Sidi Thabet, Tunisia

[c] Laboratoire ICB UMR 6303 CNRS/Université Bourgogne Franche-Comté, Dijon, France

[d] King Khalid University, Chemistry Department, College of Arts and Sciences in Mahayel Aseer, Abha, Saudi Arabia

* Corresponding authors: Dr. H. Hajji hananhajji02@gmail.com, Prof. M. Abdellaoui mohieddine.abdellaoui@gmail.com, Prof. N. Millot nmillot@u-bourgogne.fr

Abstract

The nanocrystalline hydroxyfluorapatite (HFA) was synthesized by mechanosynthesis with a planetary ball mill (PM200). The disc to jar speed ratio was constant (equal to 0.5). The effect of different milling parameters such as grinding duration, balls number's, initial powder mass and disc rotation speed were studied to apprehend their effects on both the process of grinding/mechanosynthesis and the synthesis of nanocrystalline HFA. Unlike previous studies in which milling parameters have been independently studied, the effects of these parameters on the phase contents were simultaneously studied. Abdellaoui's model was also introduced to analyse the physical milling parameters effect such as the injected shock power, the shock kinetic energy, the shock frequency and the cumulated kinetic energy on the microstructural properties and synthesized phases contents. The results predicted by the model were compared to experimental ones. This study showed that the optimal conditions for the synthesis of nanocrystalline HFA were reached when the mechanosynthesis was carried out with a speed of 450 rpm, 6 balls, 1.2 g of starting material and 24 h of grinding duration. X-ray diffraction characterization confirmed the purity phase of HFA nanocrystalline powders.

Keywords: grinding parameters, mechanosynthesis, hydroxyfluorapatite, model, optimisation.

1. Introduction

Calcium phosphate with apatite structure is of great interest in various fields such as chemical fertilizer industry, biology, health and environment. The hydroxyfluorapatite (HFA) crystallizes in the hexagonal system (with $P6_3/m$ space group) with a chemical formula corresponding to $Ca_{10}(PO_4)_6(OH)F$ (HFA) [1]. The fluorine ion F^- has an important effect on the biological and physical properties of hydroxyapatite (HA) [2]. Fluorine substituted HA (HFA) which is a biomineral that can be used as a dental and bone-implant material in the body [3],[4]. Hydroxyfluorapatite are also characterized by improved bioactivity [5] and good biocompatibility in nanocrystalline form [6],[7]. Many methods have been used to obtain hydroxyfluorapatite , such as solid-state method [8] hydrothermal reactions [9], double-decomposition method [10] and the sol-gel route [11]. Furthermore, mechanosynthesis has been used to prepare nanostructured materials that cannot be elaborated by other methods [12],[13],[14]. Mechanosynthesis is interesting due to the reduction of reaction time the obtention of nanomaterials with particular physicochemical properties and also the solid-state reaction. Indeed, mechanosynthesis makes it possible to obtain metastable phases such as supersaturated solid solutions in comparison with thermodynamically stable phases [15] or purely amorphous alloys [16],[17],[18].

During the milling process, the balls travel along displacement paths that cause friction and impact effects [18]. The planetary ball mill received more attention because of its relative simplicity [19]. The physics of mechanosynthesis could be studied at different levels. It is indeed possible to be interested on the one hand in macroscopic phenomena concerning experimental conditions, *i.e.* the energies involved, on the other hand in microscopic phenomena (on the scale of the powder particle) and finally in the atomic level [20]. Macroscopically, the global grinding parameters are the kinetic shock energy (E_{cc}, J/hit), the shock frequency (F_{shock}, Hz), the injected shock power ($P_{inj,}$ W/g) and the cumulated energy (E_{cum}, Wh/g). These grinding parameters have been defined by M. Abdellaoui *et al.*,[18],[21]. Many people have studied the impact of the milling parameters on the synthesis of several compounds

by a planetary ball mill [18],[22],[23],[24]. Nasiri-Tabrizi *et al*. [22] and Mandal *et al.* [23] studied the effect of grinding parameters such as milling time, ball diameter and ball to powder weight ratio on the hydroxyapatite formation. In particular, grinding time is a major parameter for the synthesis of nanocrystalline hydroxyapatite. This structure has been obtained after 10 h of milling as reported by Lala *et al.* [24], 15 h as reported by Zahrani *et al.* [25], 25 h as reported by Mochales *et al.* [13],[26] and 60 h as reported by Silva *et al.* [27]. Therefore, during the grinding process, the energy transferred to the powders by the balls depends on various grinding parameters, such as the dimensions and rotation speeds of disc and jars, the type of jars and balls, grinding duration, number of balls, initial powder mass and ratio of mass between the balls and the powder [28]. However, most of these reports show that the synthesis of apatite by mechanosynthesis was very time-consuming and that the mass production of powder, therefore, remains a challenge [29]. To meet all these challenges, a new efficient method has been developed for the synthesis of nanocrystalline hydroxyfluorapatite powder at room temperature. Some studies are also attempting to model the synthesis mechanism [18],[30],[31],[32]. Indeed, it is necessary to choose optimal grinding conditions and to compare the results obtained with different experimental results. Kinematic equations describing the rotation speed and the trajectory of the balls within the jar have been proposed by several models in the literature. These models suggested that the shocks between jars inner walls and balls induced energy transfer [18],[30],[33].

In the present study, both quantitative and spectroscopic analyses have been realized to evaluate the microstructural properties and the amount of hydroxyfluorapatite prepared. Then the results were combined with the injected shock power and cumulated energy values in order to show how these two parameters govern the variation of the different structural parameters. Another aim of this paper was to optimize these milling conditions to obtain the most important amount of nanoparticles of hydroxyfluorapatite. Thus, the resulting shock frequency, the injected shock power and the kinetic energy were also discussed.

2. Experimental procedure

The mechanosynthesis of HFA was carried out by a planetary ball mill Retsch PM200, using stainless steel vials of 50 mL in volume and balls from the same material of 10 mm in diameter (ϕ) and weighing about 4.051 g. The planetary ball mill consists of an angular-speed rotating plate on which two jars rotating in the opposite direction are fixed. For this planetary ball mill the disc to jar rotation speed ratio is 1:2. Both jars had a diameter of 46 mm and were placed on a disc of 248 mm in diameter. A detailed investigation was carried out to see the effect of important milling parameters like rotation speed of disc, number of balls, powder mass, ball to powder mass ratio and grinding duration. To study the effects of milling parameters, four different tests were conducted (**Table 1**). The procedure consisted in varying one parameter while keeping the other parameters constant. The first part focused on the effect of the disc rotation speed (**Ω: samples V1 to V4**, Table 1). In the second experiment, only the number of balls may vary (**Nb: samples N1 to N4**, Table 1). In the third experiment, the effect of the initial weight of powder was investigated **(mp: samples M1 to M4, Table 1**). The last part was dedicated to the variation of the milling duration (**t: samples T1 to T5**, **Table 1**). In each of the combinations mentioned in **Table 1**, the effects of the disc rotation speed, the balls number, the initial weight of powder and the milling duration were measured simultaneously. The ratio of balls mass to initial powder mass (BPR) was determined for each composition milling parameters (**Table 1**).

For the mechanosynthesis of hydroxyfluorapatite, stoichiometric amounts of calcium carbonate $CaCO_3$, diammonium hydrogen phosphate $(NH_4)_2HPO_4$ and ammonium fluoride NH_4F were used as starting reactants. The synthesis reaction proceeded as follows:

$$10\ CaCO_3 + 6\ (NH_4)_2HPO_4 + NH_4F \rightarrow \mathbf{Ca_{10}(PO_4)_6(OH)F} + 13\ NH_3 + 10\ CO_2 + 9\ H_2O \quad \text{(Eq. 1)}$$

The shocks between balls, inner jar wall and powder increased the temperature leading to the formation of gases (molecules of water, ammoniac and carbon dioxide). Therefore, a rest period of 4 min was needed to limit aggregates and gases formation.

Table 1: Summary of the milling parameters. Ω: disc rotation; Nb: number of balls; mp: mass of powder; t: milling duration. BPR: Ball to Powder weight Ratio, with m_{ball} = 4.051g, ϕ = 10mm.

Sample	Ω (rpm)	Nb	mp (g)	t (h)	BPR
V1	150	6	1.2	24	20.255
V2	250	6	1.2	24	20.255
V3	350	6	1.2	24	20.255
V4	450	6	1.2	24	20.255
M1	450	6	1.0	24	24.306
M2	450	6	1.2	24	20.255
M3	450	6	1.4	24	17.361
M4	450	6	1.7	24	14.297
N1	450	3	1.2	24	10.127
N2	450	5	1.2	24	16.879
N3	450	6	1.2	24	20.255
N4	450	7	1.2	24	23.630
T1	450	6	1.2	4	20.255
T2	450	6	1.2	10	20.255
T3	450	6	1.2	16	20.255
T4	450	6	1.2	20	20.255
T5	450	6	1.2	24	20.255

PANalytical XPERT-PRO Diffractometer system was used to determine the crystalline phase content. X-ray diffraction (XRD) was affected by CuKα radiation (λ = 1.54059 Å) with 2θ varying from 10 to 80° in steps of 0.026°. Thus, the obtained patterns were compared to the standard data file of International Centre for Diffraction Data (ICDD) Match software was used to determine the percentage of each phase *via* Rietveld refinement method [28],[34].

Brunauer-Emmett-Teller (BET) method was used to determine the specific surface area of powders by the adsorption isotherms (5-points on a Micromeritics Gemini 2380 surface area analyzer with N_2 used as the adsorbate). The out gassing was 100°C under a pressure of 20mTorr for 15h. Particle's diameter was calculated using Eq. 2 [35]:

$$D_{BET} = \frac{6000}{\rho \times A} \qquad \text{(Eq. 2)}$$

Where D_{BET} is the particle's diameter calculated in nm, ρ is the density in g/cm^3 the density in g/cm^3 here equal to $\rho = \frac{M \times Z}{N \times V}$, M is a mass molar of hydroxyfluorapatite, Z is the number of formula units in a unit cell, N is the number of Avogadro (N = 6.022 10^{23} mol^{-1}), V is the cell's volume ($V = \frac{a^2 c\sqrt{3}}{2}$) (a and c are the cell's parameters) and A : specific surface area in m^2/g.

A Spectrum Two 104462IR spectrophotometer equipped with a diamond ATR setup in the range 4000-400 cm^{-1} was used to analyze all the samples by Infrared (IR) absorption analysis.

Raman analysis was performed by the RENISHAW in Via spectrometer equipped with 50 cm^{-1} cut edge filters and an array of 1800 grooves/mm. The preparation of the powders to be analyzed was done as follows: a volume of about 5 mg was deposited on a hydrophobic and reflective solid (Tienta SpectRIM) after sonication of the concentrated suspension of NP. The recording of all the spectra was done under the same conditions such as: laser 532 nm, detector centered at 1000 cm^{-1}, laser at 10% or 1%, 100 acquisitions of 1s, objective 50).

As-prepared powders were characterized by Scanning Electronic Microscopy (SEM) *via* a JEOL JSM6400F coupled to an oxford instruments EDS analyser. Sample preparation was performed by

evaporation of a dilute suspension of nanopowder in water on a carbon-coated silicon substrate. EDS analysis of the samples was performed by selecting 5 areas with two scales of 50 µm and 1 µm. The obtained samples were analyzed by Transmission Electron Microscopy method (TEM) *via* JOEL JEM-2100F microscope (at 200 kV, point-to-point resolution of 0.19nm). The powders were prepared by evaporating a diluted suspension of NPs in water on a carbon-coated copper grid.

The thermal stability of powders was determined by Thermo-Gravimetric Analysis (TGA) TA instrument *via* an airflow rate of 25 mL/min and a temperature rate of 5°C/min from 25°C to 800°C. Measurements by X-ray photoelectron spectroscopy (XPS) were collected with a PHI 5000 Versa probe instrument equipped with an Al radiation monochromator Kα (EKα(Al) = 1486.7 eV with a 200 µm diameter spot). A sheet of indium was used to immobilize the nanoparticles during the measurements. The powders were pressed on this sheet. The Casa XPS processing and MultiPak software were used to determine the quantitative analysis of the resulted data. In order to avoid the accumulation of charges on the surface of the samples the neutralization process was applied. The O1s peak at 532.0 eV was used as an internal reference to correct the positions of the XPS peaks. A Shirley background was subtracted and the Gauss (70%) - Lorentz (30%) profile was used. The total width at half height (FWHM) was set between 1.5 and 2.0 eV.

Hydrodynamic diameter of all samples was determined with the Dynamic Light Scattering (DLS) method (at 25°C with a Malvern Nano ZS instrument supplied by DTS Nano V7.02 software). The first step taken, prior to measurement is that, each suspension of sample was diluted in an aqueous solution containing NaCl (10^{-2}M). The suspension underwent a pulsed ultrasound treatment for 3 min at a power of 375W with Sonics Vibra Cells. DLS curves were derived from intensity calculations at pH = 7. For each sample, the DLS measurements were repeated thrice.

3. The kinematic model of the planetary ball mill

Abdellaoui *et al.* [18] developed a mathematical model which advantage is to highlight the physical parameters that govern the formation and/or transformation phase induced by the mechanosynthesis. According to this model, the formation and/or transformation phase is governed only by the injected shock power which is the product of the kinetic shock energy by the shock frequency [18]. Abdellaoui *et al.* [18],[36] showed that the trajectory of a ball can be summarized in four steps which are the rolling of the ball on the wall of the jar, the removal of the ball from the wall, the course in the jar and the impact on the wall of the jar.

As stated in this model [18], the contents of the formed phases depend on the cumulated kinetic energy (E_{cum}) which is the product of the injected shock power (P_{inj}) and the grinding duration(t).

$$E_{cum} = P_{inj} \times \mathrm{t} \qquad \text{(Eq. 3)}$$

The injected shock power (P_{inj}) is given by the ratio of the total power (P_{tot}) to the initial mass of the powder (mp).

$$P_{inj} = \frac{P_{tot}}{mp} \qquad \text{(Eq. 4)}$$

The total power is the product of the shock kinetic energy (E_{cc}) by the total shock frequency (f_{tot}).

$$P_{tot} = E_{CC} \times f_{tot} \qquad \text{(Eq. 5)}$$

The total shock frequency (f_{tot}) is given as follows:

$$f_{tot} = F_{shock} \times \mathrm{Nb} \qquad \text{(Eq. 6)}$$

Where F_{shock} (Hz) is the shock frequency of an individual ball and Nb is the number of balls.

The kinetic shock energy is given as follows:

$$E_{CC} = \frac{1}{2} m_b V_{shock}^2 \qquad \text{(Eq. 7)}$$

Where m_b is the ball weight and V_{shock} is the velocity of the ball at the shock event.

It is worth mentioning that the above equations regroup all the machine variables implicated in mechanosynthesis process. Preceding equations have been utilized to calculate the cumulated kinetic energy transmitted by the balls to the powders during milling process in a Restch PM200. Kinetic shock energy (E_{cc}) and shock frequency per ball (f_{chock}) are determined using the software developed by Abdellaoui *et al*. [18]. The technical parameters used in the following calculations are: disc radius (124 mm), the jar radius (23 mm), radius of the balls (5 mm), rotation speeds of disc and the jar.

3.1. Effect of the rotation speed of disc

Fig. S2 (Table S1) shows the effect of disc rotation speed on the kinetic shock energy, injected shock power, and shock frequency. Balls number was considered equal to 1 and the powder weight was equal to 1 g. This figure shows that the shock frequency increases linearly with the increasing of the disc rotation speed. Nevertheless, the kinetic shock energy increases progressively. These behaviors are similar to that suggested by Chattopadhyay *et al*. [37]. So, as the injected shock power is the product of the kinetic shock energy by the shock frequency (Eq. 5), the injected shock power increases progressively while increasing the disc rotation speed and follows the same trajectory of the kinetic shock energy. The value of injected shock power reaches 1.6 W/g for 450 rpm disc rotation speed.

3.2. Effect of the number of balls

Fig. S3 (Table S1 and Table S2) shows the variation of the injected shock power and the shock frequency for different balls numbers (3, 5, 6 and 7 balls). Based on the model, for a rotation speed of disc that is equal to 450 rpm and 1 g of powder, both the injected shock power and the shock frequency increase linearly when raising balls number (Eq. 4, 5 and 6).

According to Eq. 4, the injected shock power can be increased either by increasing the total power or by decreasing the mass of the powder with a constant balls number. Indeed, the total power increases

when increasing the kinetic shock energy and/or the total shock frequency. The shock frequency is proportional to the number of balls. The kinetic shock energy increases when increasing the ball weight or the disc rotation speed (detailed equations in reference [18]). Nevertheless, the total shock frequency increases when increasing the disc rotation speed or the ball number. In this context, when increasing the ball number from 1 to 7, the total shock frequency value increases from 17.26 Hz to 120.82 Hz and the injected shock power increases from 17.26 to 120.82 W/g.

Consequently, according to this model [18], wherever the injected shock power increases with the balls number, the cumulated kinetic energy (E_{cum}) increases in the same manner (Eq. 3).

3.3. Effect of initial powder mass on the injected shock power

Fig. S4, Table S1 and Table S2 show that, when keeping the disc rotation speed and the ball number constant, the injected shock power decreases once the initial powder mass increases (Eq. 4). Similarly, the cumulated kinetic energy will be inversely proportional to the initial mass of powder and will decrease when the mass of powder increases.

To achieve a critical injected shock power value able to induce a new phase formation, starting from initial precursors, we have to increase the total power or to decrease the sample mass. Indeed, the total power increases with the increasing of the kinetic shock energy increases or the total shock frequency increases. The kinetic shock energy rises as the mass of the ball increases or the disc rotation speed increases. Thus, the easier way to increase the injected shock power and then the cumulated kinetic energy is by decreasing the powder mass value.

4. Results and discussion

Optimization and modeling of grinding parameters is very important to obtain the desirable phase and the efficient milling. The effective milling parameters, other than the technical parameters such as the disc radius and the vial radius, are the disc rotation speed, the ball radius, the ball mass, the number of

balls, the initial mass of powder and the grinding duration. Beside the technical and cinematic parameters, the material of grinding balls greatly affects the formation of products in mechanochemical processes. Therefore, at the beginning of this work, HFA was synthesized by varying the type of ball material: stainless steel, agate and alumina with 450 rpm, 6 balls, 1.2 g and 24 hours. The X-ray diffractograms of the three samples (**Figure 1**) show that the apatite proportions are lesser for agate and alumina balls than for stainless balls and therefore, stainless-steel balls are chosen to achieve this work. For ball diameter, Eq. 7 illustrates that E_{CC} increases when the ball mass m_b increases and consequently when the ball diameter increases for a given ball material. So, the injected shock power and the cumulated energy increase when increasing the ball radius. In our previous works [38] , we reported that balls with 10 mm radius are suitable for the degree of filling of the jars and the grinding efficiency. Thus, in the rest of this work, stainless steel balls with a radius of 10 mm is used.

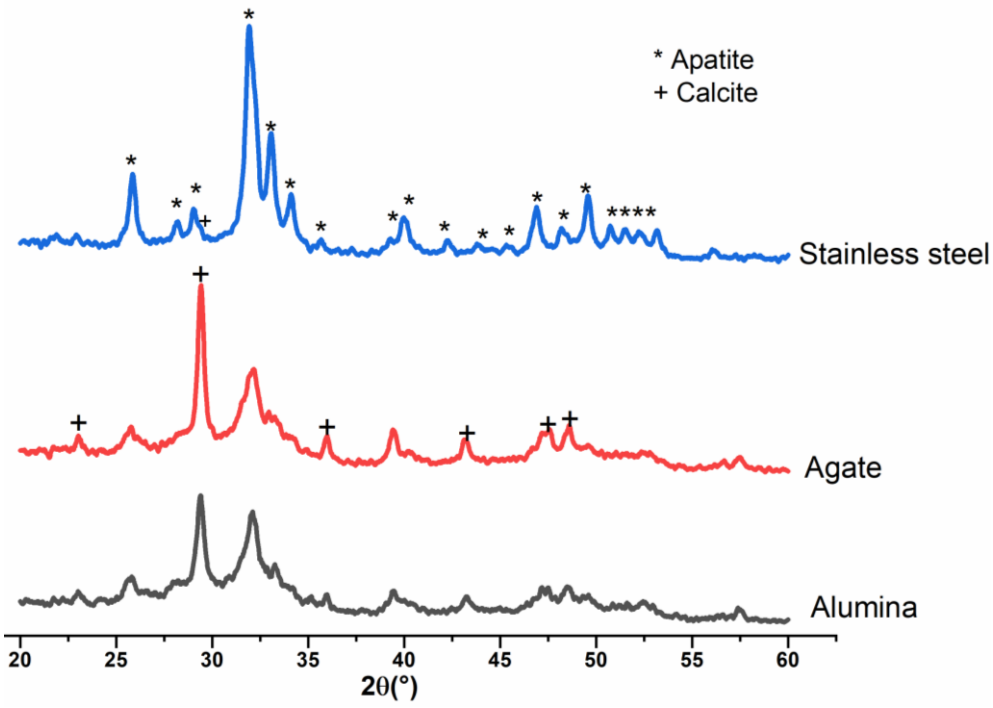

Figure 1: XRD of HFA powders as a function of ball material type

Table 2 shows the values of the injected shock power and the cumulated energy corresponding to the different grinding parameters. The apatite and calcite contents, the particle diameter D_{BET}, the

specific surface area and the hydrodynamic diameters D_H are also listed as function of the milling conditions.

Table 2. Milling conditions and physicochemical properties of the obtained HFA with m_{ball} = 4.051g, ϕ = 10mm. D_{BET} is the diameter inferred from specific surface (A). D_H is the hydrodynamic diameter, measured in water [NaCl] 10^{-2} M, at pH 7.

Variable	**Sample**		**P_{inj} (W/g)**	**E_{cum} (Wh/g)**	**Apatite %**	**Calcite %**	**D_{BET} (nm)**	**A (m^2/g)**	**D_H (nm)**
Ω (rpm)	V1	150	0.31	7.38	57.9 ± 0.3	42.1 ± 0.2	40 ± 1	23.6 ± 0.2	762 ± 55
	V2	250	1.43	34.21	60.5 ± 0.4	39.5 ± 0.2	33 ± 1	28.2 ± 0.2	768 ± 56
	V3	350	3.91	93.89	88.8 ± 0.3	11.2 ± 0.2	28 ± 1	33.1 ± 0.3	1151 ± 90
	V4	450	8.32	199.58	99.6 ± 0.3	0.4 ± 0.1	24 ± 1	38.7 ± 0.3	1246 ± 10
mp (g)	M1	1.0	9.98	239.47	99.8 ± 0.2	0.2 ± 0.1	23 ± 1	41.3 ± 0.2	1320 ± 19
	M2	1.2	8.32	199.56	99.6 ± 0.3	0.4 ± 0.2	24 ± 1	38.7 ± 0.3	1246 ± 10
	M3	1.4	7.13	171.05	79.3 ± 0.4	20.7 ± 0.3	25 ± 1	37.6 ± 0.2	1170 ± 90
	M4	1.7	5.87	140.86	68.4 ± 0.6	31.6 ± 0.1	25 ± 1	37.0 ± 0.3	857 ± 12
Nb	N1	3	4.12	99.78	93.0 ± 0.1	7.0 ± 0.2	35 ± 1	27.4 ± 0.2	929 ± 12
	N2	5	6.93	166.30	95.6 ± 0.2	4.4 ± 0.1	27 ± 1	34.9 ± 0.2	992 ± 12
	N3	6	8.32	199.56	99.6 ± 0.3	0.4 ± 0.1	24 ± 1	38.7 ± 0.4	1246 ± 10
	N4	7	9.70	232.80	98.7 ± 0.3	1.3 ± 0.1	20 ± 1	46.5 ± 0.3	1287 ± 12
t (h)	T1	4	8.32	33.26	25.2 ± 0 .1	76.9 ± 0.4	51 ±1	18.3 ± 0.1	823 ± 64
	T2	10	8.32	83.15	32.5 ± 0.2	68.5 ± 0.2	44 ± 1	20.9 ± 0.1	842 ± 11

	T3	16	8.32	133.04	35.9 ± 0.2	36.1 ± 0.2	45 ± 1	21.0 ± 0.1	961 ± 99
	T4	20	8.32	166.3	52.5 ± 0.3	47.5 ± 0.2	38 ± 1	24.8 ± 0.5	1214 ± 2
	T5	24	8.32	199.56	99.6 ± 0.3	0.4 ± 0.1	24 ± 1	38.7 ± 0.3	1246 ± 10

4.1. Modeling and effect of grinding parameters on the microstructural state of the prepared product

4.1.1. Effect of the disc rotation speed

The initial powder mass (mp) was kept constant and equal to 1.2 g when the milling duration was equal to 24 h. 6 balls (m_{ball} = 4.051 g, ϕ = 10 mm) were used. The XRD patterns of the HFA samples, prepared with different values of disc rotation speed such as 150, 250, 350 and 450 rpm, are shown in **Fig. 2 (a)**.

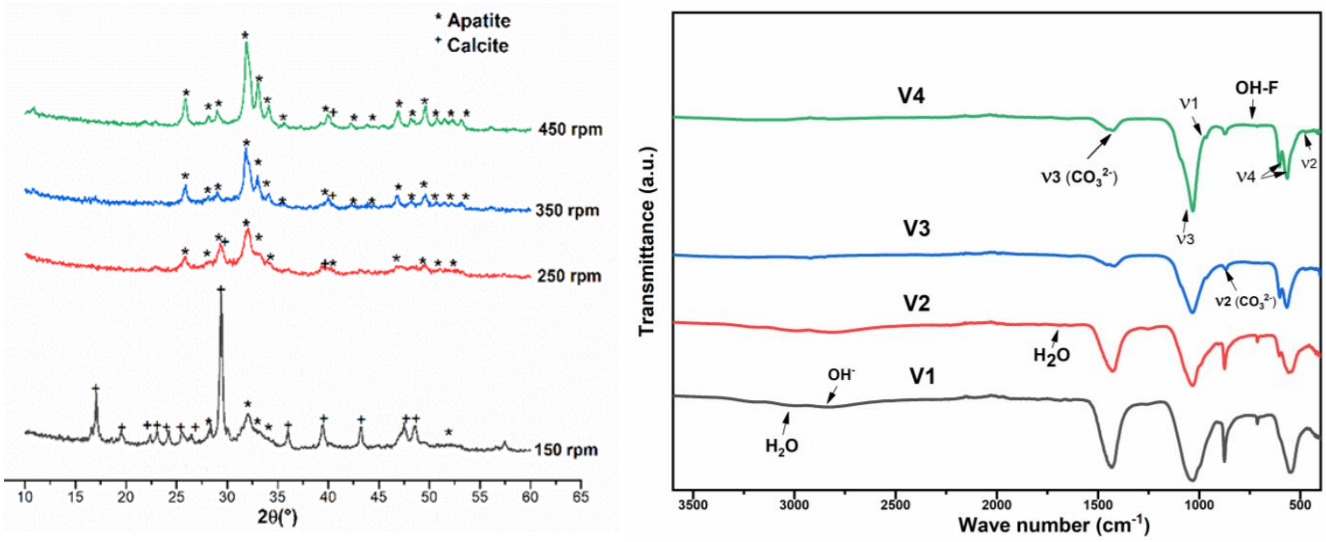

(a) **(b)**

Fig. 2 (a) XRD patterns of synthetized samples as a function of the disc rotation speed (mp =1.2g, 6 balls and 24 h); (b) IR spectra of samples prepared at different disc rotation speed (a. u. arbitrary units)

XRD patterns show the presence of the apatite phase, whose peaks could be crystallized in hexagonal system (space group $P6_3/m$), with respect to hydroxyfluorapatite (HFA: ICDD # 96-210 4756) (**Fig. 2 (a)**). Also, supplementary peaks are detected and assigned to unreacted carbonate calcium ($CaCO_3$) with ICDD card: #00-00-005-0586. The percentages of these two phases considering the different values of disc rotation speed are given **Table 2**. At a speed of 150 rpm, powder mixture consists mainly of HFA and calcite (present in the same proportions). At 250 rpm, the peaks attributed with the calcite phase decrease in intensity. XRD diffractogram of the V3 sample (350 rpm) indicates that the HFA phase is the principal phase and only a very low amount of calcite is observed. For a speed equal to 450 rpm, there is a clear improvement in crystallinity of the HFA phase and absence of calcite lines. The apatite lines become more defined, thinner and intense as the disc rotation speed increases indicating an improvement in the crystallinity and an increase of the content of the obtained HFA phase. It is important to note that when the disc rotation speed increases from 150 to 450 rpm, the injected shock power increases from 0.31 W/g to 8.32 W/g and the cumulated energy increases from 7.38 Wh/g to 199.58 Wh/g (**Table 2**). The increase in the cumulated energy induces a proportional increase of the percentage of prepared HFA phase from 57.9% to 99.6% (**Table 2**).

Fig. 2 (b) shows the IR spectra of all samples. The absorption bands assigned to phosphate groups PO_4^{3-} at about 1010-1156 cm^{-1} ($\upsilon 3$: asymmetric elongation mode), 955-966 cm^{-1} ($\upsilon 1$: symmetric elongation vibration mode), 631-591 cm^{-1} ($\upsilon 4$: symmetric deformation mode) and at 468-575 cm^{-1} ($\upsilon 2$: asymmetric deformation vibration mode) are observed in all IR spectra. The band at 667 cm^{-1} is attributed to the bending mode of OH^- (υL: symmetric elongation vibration mode). All IR spectra show the appearance of a band around 3000-3425 cm^{-1} attributed to the stretching mode of structural hydroxyl (OH(υs)) [28]. Moreover, the vibration band at 713 cm^{-1} is assigned to OH-F interaction is observed. This result suggested that F^- ions have partially replaced hydroxyl ions in the HFA structure, as shown for similar works [10],[39]. In the region 2500-3700 cm^{-1} and at 1640 cm^{-1}, the water-induced bands are observed. The bands at 875 cm^{-1} are attributed to the residual NH_4^+ [40]. Besides, IR

spectrum confirms the presence of carbonate bands appearing in the range of 1400-1538 cm^{-1} (υ3: elongation antisymmetric modes (in doublet form)) and 872-880 cm^{-1} (υ2: the off-plane bending mode (in singlet form)) resulting from the calcite phase that did not react as observed by XRD [41],[42],[43]. The intensity of the bands of the carbonate group decreases when increasing disc rotation speed (sample V1 to sample V4). This result can be correlated to the decrease of the calcite content as the disc rotation speed increases. In addition, by increasing the disc rotation speed, the phosphate group absorption bands become more defined and the four modes become more observed. Moreover, the increase of the disc rotation speed induces the decrease of the intensity of the water absorption band around 2800-3500 cm^{-1}. In fact, increasing the disc rotation speed leads to the increase of the choc numbers in the jar. The elevation of the temperature can explain the departure of adsorbed water [23]. The IR results totally agree with the XRD ones and showed the increase of the apatite content and the decrease of the calcite content when increasing the cumulated energy by increasing the injected shock power due to the increase of the disc rotation speed (**Table 2**).

Fig. 3 indicates the Raman spectra of the same samples prepared at different disc rotation speed. Raman spectroscopy is more sensitive to secondary phase as compared to XRD and IR [44]. The ν1(PO_4^{3-}) mode at 960-962 cm^{-1}, characteristic of pure HFA, is the most intense in all Raman spectra, as shown in **Fig. 3 (a) and (b)**. This mode is associated with the fully symmetrical P-O-P stretching mode (ν1) of the free tetrahedral phosphate ion. A part from that the intensity increases as the disc rotation speed increases, showing an increase of the apatite content in agreement with the XRD and IR results. The vibration modes ν2, ν3 and ν4 of the phosphate group are observed in all Raman spectra for the HFA phases obtained at different disc rotation speeds (samples V1, V2, V3 and V4). All the bands attributed to the vibration modes of carbonate group are also detected (**Fig. 3).** A shoulder peak at 588 cm^{-1} and the peaks at 614 cm^{-1}, 589 cm^{-1}, 611 cm^{-1} are attributed to PO_4^{3-} vibration modes (ν4) (asymmetric mode of O-P-O bending) [45],[46]. As the disc rotation speed rises, we notice a peak disappearance around 710 cm^{-1}, 782-793 cm^{-1}, 878 cm^{-1}, 1110 cm^{-1}, 1210 cm^{-1} and 1269-1377 cm^{-1}

vibration modes attributed to the carbonate group [28],[47]. The intensities of the calcite vibration bands increase whenever the disc rotation speeds are increased. These results do thoroughly go hand in hand with the results obtained by XRD and IR spectroscopy.

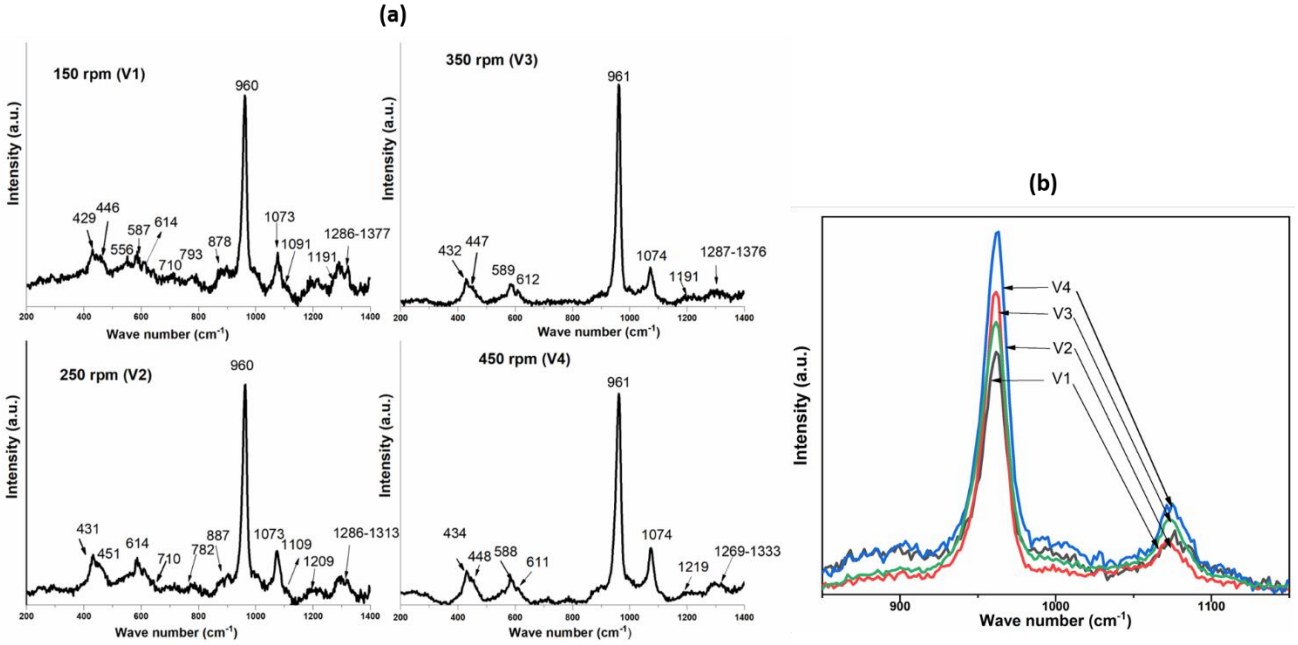

Fig. 3 (a) Raman spectra of hydroxyfluorapatite samples obtained at 150, 250, 350 and 450 rpm disc rotation speeds; (b) zoom on the PO_4^{3-}(υ1) and calcite (υ3) vibration modes (a. u. arbitrary units)

Fig. S5 shows that the cumulated kinetic energy, the injected shock power, the apatite phase content and the surface specific area (A) increase when the disc rotation speed increases. The BET size, D_{BET}, decreases from 40 nm to 24 nm when the disc rotation speed increases from 150 to 450 rpm. The hydrodynamic diameter obtained by the DLS analysis has the inversely tendency as the D_{BET}. Additionally, the hydrodynamic diameters (D_H) in water obtained for all samples confirm that all the prepared powders are aggregated (**Table 2**). It can be observed that a high disc rotation speed leads to larger sized aggregates. Simultaneously, agglomeration in the liquid, during DLS measurements, may be promoted by Van der Waals force holding particles together [48].

The increase in disc rotation speed increases the shocks number between the jar wall and the balls and the intensity of the shock velocity, resulting in an increase in the kinetic shock energy and the shock frequency of the balls and so the increase of the injected power as it is shown in **Fig. S5**. Abdellaoui *et al.* [18], have shown that shocks between the jar wall, the balls and initial powder mass can induce an increase of the powder temperature and the milling medium inducing an increase of the calorific energy of the initial powder, yet this increase is not sufficient to induce the formation of new phases or the increase of their content. With reference to [18], the new phase formation proceeds above a minimum injected shock power input and below a certain maximum injected shock power input. For low values of injected shock powers, the precursors free energy of the precursors resulting from the increase of the concentration defect induced by plastic deformation, is not high enough to induce the formation of a new phase. Therefore, the precursors input do not react at such injected shock powers. The powders grain size decreases with the increase of the milling duration. However, for a medium injected shock power level, a new phase is able to be formed. In fact, for this medium shock power level, the free energy of the new phase ($\Delta Gc(HFA)$) is lower than the free energy of the mixture of the precursors, as explained by Eq. 8 [49]:

$$\%\ A x \Delta G_c(A) + \%\ B\, x \Delta G_c(B) + \%\ C\ x \Delta G_c(C) + \Delta G_{defect}\,(A, B, C) > \Delta G_c(HFA) \quad \text{(Eq. 8)}$$

where A= $CaCO_3$, B= $(NH_4)_2HPO_4$, C= NH_4F, ΔGc is the free energy of the crystalline phase and ΔG_{defect} is the increase in the free energy due to the defects introduced by mechanical milling [18]. ΔG_{defect} increases by increasing the injected shock power. Therefore, based on this model, the formation of new phases is governed by the value of the injected shock power and the content of the new phase is proportional to the cumulated energy value. The results reported in **Fig. S5.** are in agreement with the theoretical model. In fact, they showed that *i)* the formation of the new phase HFA occurs for a medium value of injected shock power and *ii)* the HFA phase content increases with the increasing of the cumulated energy.

As reported in the model [18], for a constant milling time, the increase of the cumulated energy is due to the increase of the injected shock power (Eq. 3). However, as the powder weight is constant, the increase of the injected shock power is due to the increase of the total shock power (Eq. 4) which is induced by the rise in the kinetic shock frequency and/or the kinetic shock energy (Eq. 5). As the ball number and weight are constant, the increase of either the kinetic shock energy or the kinetic shock frequency is due to the increase of the disc rotation speed (Eq. 6 and 7). That may be the reason why the HFA content increases compared to the calcite content conjointly with the disc rotation speed. The evaluation of the injected shock power P_{inj}, cumulated energy E_{cum} computed as a function of the disk rotation speed in the present analysis show logical agreement with the values of the same parameters reported in the literature [14],[50]. Indeed, it is clear from **Fig. 3** that the results obtained from the present analysis is in good agreement with that suggested by Chattopadhyay *et al.*[37] despite a slight difference in the method of calculation of physics parameters (P_{inj}, E_{cum}). In this reference the *ab initio* calculations are used. Structural analyses show that under these milling conditions, the use of a 450 rpm disc rotation speed allows to reach an E_{cum} value of 199.58 Wh/g which is the value required to produce 99.6% of HFA.

4. 1. 2. Effect of the initial powder mass

The disc rotation speed and the milling duration are kept constant at 450 rpm (the optimal value according to the previous paragraph) and 24 h, 6 balls (m_{ball} = 4.051g, ϕ = 10mm) are used. XRD patterns of hydroxyfluorapatite synthesized for different values of initial powder mass are presented in **Fig. 4 (a)**. The mass of the powder considered for the performed tests are 1, 1.2, 1.4 and 1.7 g. Most peaks can be indexed in the hexagonal system (space group: $P6_3/m$) assigned to hydroxyfluorapatite (ICDD card#96-210 4756) (**Fig. S1**). However, other peaks can be indexed in the trigonal system with the space group R3m, they are assigned to the calcite phase (ICDD card #00-00-005-0586). The calcite phase is present in all synthesized HFA samples. HFA diffractograms show that the apatite peaks are

more intense and defined for 1 and 1.2 g. However, those of the calcite phase, almost absent for 1 and 1.2 g, are well defined for 1.4 and 1.7 g. In other words, with low values of the initial mass of powders, the apatite peaks are more defined, thin and intense. It is important to note that when the initial mass of powder increases from 1 to 1.7 g, the injected shock power decreases from 9.978 W/g to 5.869 W/g and the cumulated energy decreases from 239.47 Wh/g to 140.86 Wh/g (**Table 2**). This decrease of the cumulated energy induces a proportional decrease of the content of the formed HFA phase from 99.8% to 68.4% and a proportional increase of the calcite content from 0.2 to 31.6% (**Table 2**). These results corroborate those reported by Hajji *et al.* [28].

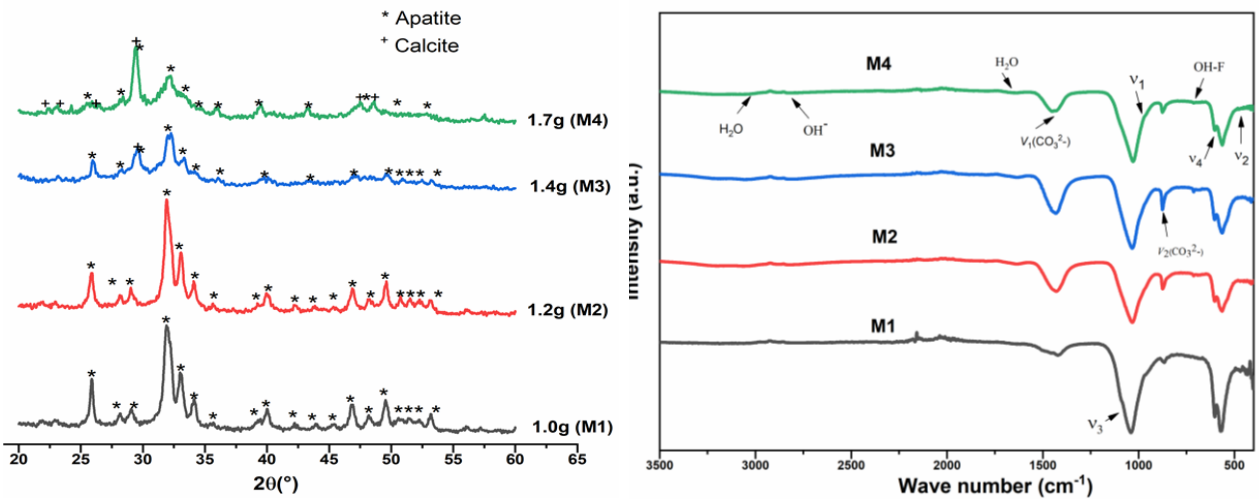

(a) **(b)**

Fig. 4 (a) XRD patterns of synthesized samples as function of the initial powder mass (mp) with Ω = 450 rpm, 6 balls and 24 h; (b) IR spectra of samples prepared at different initial mass of powder (mp) (a. u. arbitrary units)

Fig. 4 (b) indicates the IR spectra of hydroxyfluorapatite powders synthesized with different values of the initial powder mass (M1-M4). All IR spectra show the presence of phosphate group vibration modes (υ1, υ2, υ3 and υ4) and the absorption bands presence attributed to the carbonate group around 868 and 1458 cm^{-1}. Thus, the four absorption bands characteristic of phosphate ions PO_4^{3-} are presented around 961 (υ1), 1120 (υ3), 520 (υ2) and 550 (υ4) cm^{-1}. The band intensity at 603-640 cm^{-}

^{1}, attributed to the bending mode of OH^- decreases whenever the initial powder mass decreases. Wide absorption bands between 3000 and 3700 cm^{-1} are observed on all IR spectra, indicating the presence of water molecules. When the value of the initial mass of powder increases, the intensities of absorption bands for PO_4^{3-} ion decrease and become poorly defined. On the other hand, the absorption bands attributable to carbonate groups become more defined and more intense. These observation is explained by the increasing of the initial powder mass which increases the degree of filling and leads to a low ball's mobility inside of the jar [50]. Furthermore, we notice the appearance of intense absorption bands around 1600 cm^{-1} attributed to the vibration of water molecules [10]. Increasing the initial powder mass decreases the mobility of balls in the jar and as a result, energy transfer is reduced. In these conditions, the molecules of adsorbed water remain within the prepared powder [28].

Fig. 5 shows the Raman spectra of the samples synthesized with different initial mass of powder. As shown in **Fig. 5 (a)** and **(b)**, the same vibration modes of various groups such as PO_4^{3-}, Ca-PO_4, CO_3^{2-} and OH^- presented in **Fig. 3** are also observed for different values of the initial mass of powder. A prominent peak at 961-962 cm^{-1}, assigned to the PO_4^{3-} vibration mode (ν1), appears. The intensity of this peak is the same in all spectra. The peaks at 447-458 cm^{-1} and 430-432 cm^{-1} correspond to the PO_4^{3-}vibration modes (ν2) and the peaks at 1074-1075 cm^{-1}, 1047 cm^{-1}, 1029 cm^{-1} correspond to the PO_4^{3-} vibration modes (ν3) [28]. Vibration modes (PO_4^{3-} ν4) at 601 cm^{-1} and peaks at 615 cm^{-1}, 590 cm^{-1} and 579 cm^{-}1 are observed. If we increase the initial powder mass, we notice the appearance of a peak around 1100 cm^{-}1 attributed to the carbonate group and of peaks around 157, 288, 709-750 cm^{-1} attributed to the calcite vibration modes [45],[51],[52],[53]. The initial powder mass increases of the carbonate vibration bands intensities.

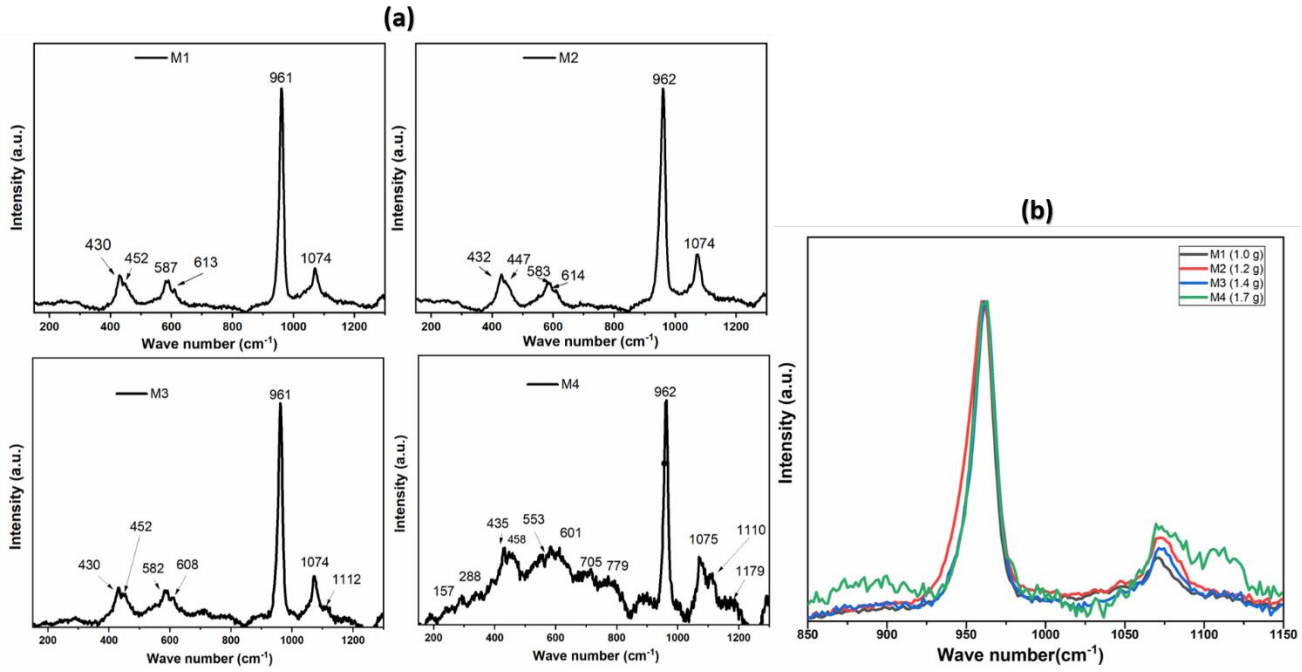

Fig. 5 (a) Raman spectra of samples prepared at different initial mass of powder (mp); (b) zoom on the PO_4^{3-} (v4) and calcite (v1) vibration peaks (a. u. arbitrary units)

The BET analysis shows that raising the initial powder mass decreases the specific surface area (**Fig. S6**, **Table 2**). The specific surface area obtained in this case increases from 37.0 ± 0.3 m^2/g to 41.3 ± 0.2 m^2/g when the injected shock power and the cumulated energy increase respectively from 5.87 W/g and 140.86 Wh/g to 9.98 W/g and 239.47 Wh/g. Therefore, D_{BET} decreases slightly from 25 nm to 23 nm when the injected shock power and the cumulated energy increase respectively from 5.87 W/g and 140.86 Wh/g to 9.98 W/g and 239.47 Wh/g in the meantime. The hydrodynamic diameter obtained by the DLS analysis has the same tendency as the specific surface area (**Table 2**). Indeed, initial powder mass decreases the size of aggregates and increases the injected shock power and cumulated energy to reach a value of 1320 nm for 9.978 W/g and 239.4 Wh/g. This high D_H value proves the aggregation of all samples (ultrasound are not able to disperse them), a very usual phenomenon for powders obtained by mechanosynthesis [54].

Fig. S6 shows that the cumulated kinetic energy, the injected shock power, the apatite phase content and the specific surface area (A) decrease if we increase the initial powder mass. As shown

previously, and referring to the used model [18], the content of the formed phase (apatite) is proportional to the cumulated energy value. These results are matching the theoretical model. In fact, the formation of the new HFA phase occurs for a medium value of injected shock power and its content decreases if we lower the cumulated energy resulting from the initial powder mass increase as shown in Eq. 3 and 4.

4. 1. 3. Effect of the number of balls

X-ray diffractograms of hydroxyfluorapatite powder synthesized by mechanosynthesis for different ball's number are given in **Fig. 6 (a)**. The samples are synthesized with a 450 rpm disc rotation speed, a 1.2 g of initial powder mass and 24 h of milling. Four different number of balls are selected; namely 3, 5, 6 and 7 balls. The XRD patterns show the presence of both the calcite and apatite phases. Thus, the majority of peaks (hexagonal system, $P6_3/m$) are related to the HFA phase. The other peaks are indexed in a trigonal system and are related to the calcite phase. When the ball's number increases from 3 to 6, the injected shock power increases from 4.16 W/g to 8.32 W/g and the cumulated energy increases from 99.78 Wh/g to 199.56 Wh/g (as listed in **Table 2**). This increase of the cumulated energy induces a proportional increase in the percentage of obtained HFA phase from 93.0% to 99.6% and a proportional decrease of the calcite content from 7.0 to 0.4% (**Table 2**). For upper number of balls (Nb=7), even the values of the injected shock power and the cumulated energy are higher, the content of the apatite phase slightly decreases to 98.7% and the content of the calcite phase slightly increases to 1.3%. This decrease of the apatite content is due to filling the jars with the balls. In fact, when the filling degree exceeds a critical value, the balls are no longer able to carry out their theoretical movement corresponding to the calculated frequency. Thus, the actual value of the shock frequency should be slightly lower than the calculated value. This induces a reduction in the real value of the injected shock power because of the cumulated energy. It is for this reason that the content of the apatite phase decreases slightly to 98.70%. Indeed, we have demonstrated that the balls' number has an

important impact on the content of apatite [22],[23],[28]. But regarding the complexity of the process, modelling [18] is made for a single ball and is generalized on a higher number, resulting in the impossibility to calculate the exact number of balls leading to this phenomenon.

The BET analyses (**Table 2**) show that the increase of the balls' number increases the specific surface area (A) , *i.e.* when increasing P_{inj} and E_{cum}. In other words, D_{BET} decreases with the increase of P_{inj} and E_{cum}. D_H obtained by the DLS analysis and A has the same tendency. It means that increasing the balls number increases the aggregates size. Therefore, it goes up with the increase of both the injected shock power and cumulated energy.

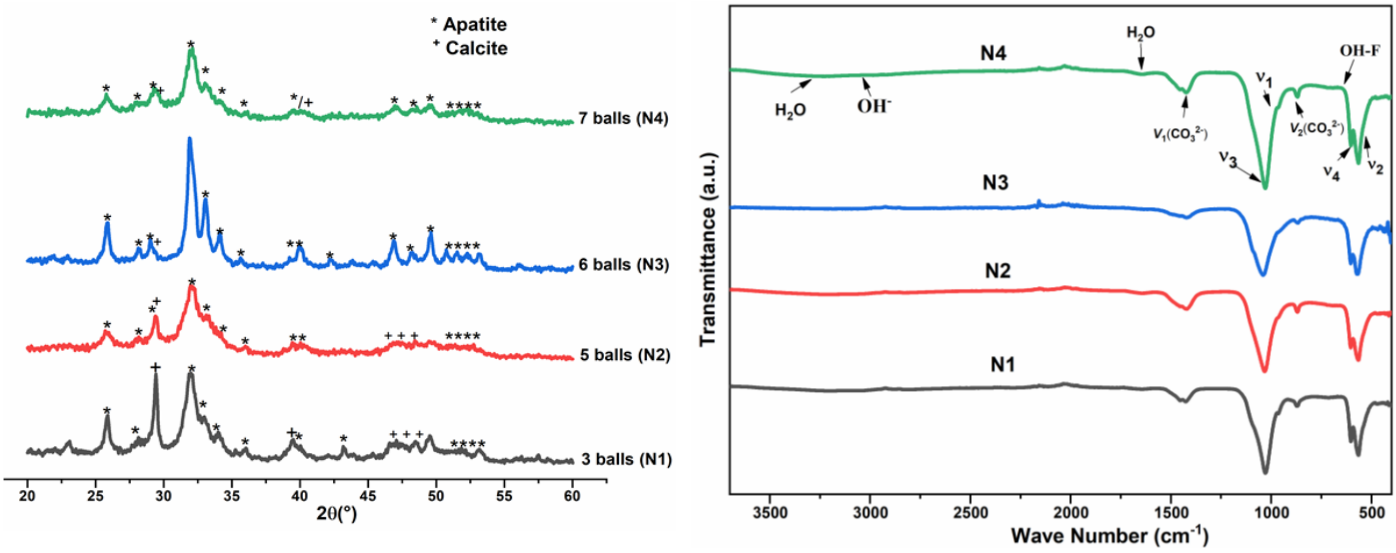

(a) **(b)**

Fig. 6 (a) XRD patterns of synthesized samples as function of the ball number's (Ω = 450 rpm, mp = 1.2g and 24 h); (b) IR spectra of samples prepared at different number of balls (Nb) (a. u. arbitrary units)

Fig. 6 (b) shows the IR spectra of hydroxyfluorapatite powders synthesized with different number of balls. All samples exhibit similar peaks characteristic and are very similar to that obtained in **Fig. 2 (b)** and **4 (b).** The bands intensity assigned to phosphate groups PO_4^{3-}(located around 962 cm^{-1}) in apatite seems to be the most intense for 6 balls. Therefore, the results obtained by IR are totally

matching those obtained by XRD and show that using 6 balls is optimal for obtaining high content of apatite phase.

Raman spectra of the synthesized samples at different number of balls are regrouped in **Fig. 7**. The same vibration modes as reported in the previous paragraphs are observed in all synthesized samples for different values of the number of balls. All Raman spectra showed the same vibration modes obtained by the **Fig. 3** and **Fig. 5**. The same vibration bands are presented but with a different in their intensity, depending on the number of balls. The intensities of these peaks are higher for a number of balls equal to 6. The peak around 1114 cm^{-1} attributed to the vibration of carbonate group clearly appears with the increase of the number of balls [23],[28],[55]. Also, the increase of balls' number raises the intensities of the carbonate group bands. It is worth mentioning that, for a number of balls equal to 7, the mobility of balls within the jar decreases, leading to the decrease of the apatite phase percentage. Ghayour *et al*. [50] suggested that increasing balls number results two important events occur. Mainly, the low mass of ball decreases their kinetic energy and a consequent reduction in energy transfer or milling efficiency. In addition, the mobility of the balls inside the jar during synthesis becomes more difficult as the degree of the filling of the jar increases, therefore their kinetic energy are also reduced. These results are in agreement with the results obtained by XRD and IR.

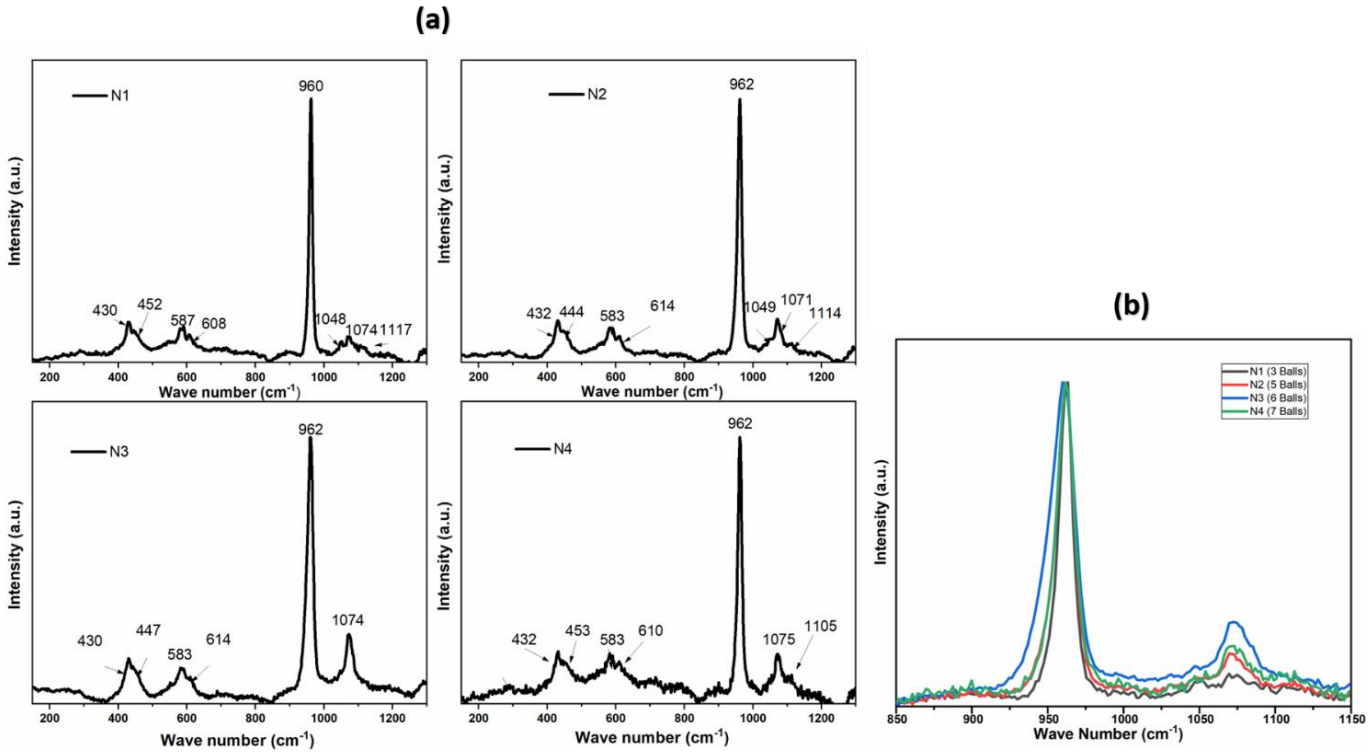

Fig. 7(a) Raman spectra of samples prepared at different number of balls and (b) zoom on the PO_4^{3-} (v4) and calcite (v1) vibration peaks (a. u. arbitrary units)

Fig. S7 shows that the cumulated kinetic energy, the injected shock power and the specific surface area increase with increasing number of balls. Moreover, apatite phase content increases to reach its maximum (99.6%) for 6 balls. The decrease of the apatite content is explained by a decrease of the real value of the cumulated energy induced by the decrease of the shock frequency related to the degree of filling of the jars with the balls explained above. So, the results reported in **Fig. S7** are in agreement with the theoretical model [18].

4. 1. 4. Effect of the grinding duration

According to the literature, there is an effect of milling duration on the apatite synthesis [22],[23],[28]. Authors revealed the high importance of this parameter and its great impact on the final composition and structure. However, many studies show that the elaboration of HA by the mechanical alloying method takes place in a high grinding time, that is why the mass production of HFA powder

remains a challenge. For instance, Nasiri-Tabrizi *et al.* [22] deduced that the increasing of the milling time leads to the increasing of the lattice strain and decreasing of the crystallite size, but the rate of both variations decreases. On the other hand, Mandal *et al.* [23] has synthesized the hydroxyfluorapatite as a function of grinding duration and demonstrated that increasing the grinding duration the value of Ca/P approaches towards the ideal (1.67) value and after 15 h of milling it attains the desired value *i.e.* 1.663. In our study, five milling durations were chosen, namely 4h, 10h, 16h, 20h and 24h. For all samples, rotation speed of disc, initial powder mass and the number of balls is kept constant equal respectively to 450 rpm, 1.2 g and 6 (optimum conditions found in the previous paragraphs). These conditions correspond to an injected shock power equal to 8.32 W/g. **Fig. 8 (a)** shows the X-ray diffractograms of HFA samples (**T1** to **T5**) synthesized at different milling durations. As previously observed, some peaks of the XRD diffractograms are indexed in the hexagonal system with the space group $P6_3/m$ and correspond to the apatite phase. The other peaks are indexed in the trigonal system and correspond to the calcite phase. According to XRD patterns, the apatite peaks become more defined, thinner and more intense once increasing the grinding duration. This is due both to the improvement in crystallinity and to the increase of the apatite content. Moreover, the intensities of calcite peaks decrease when we increase the milling duration. In fact, after 4 h of milling, the XRD diagrams show that the $CaCO_3$ peaks are very intense and those of the apatite phase are very weak. After 10 h of milling, broad and weak characteristic peaks of the apatite phase, located around 31.7-33.71°, appear. After 20 h of milling, the HFA peaks become more intense and more defined. After 24 h of milling, apatite peaks become more defined and more intense and the calcite ones completely disappear.

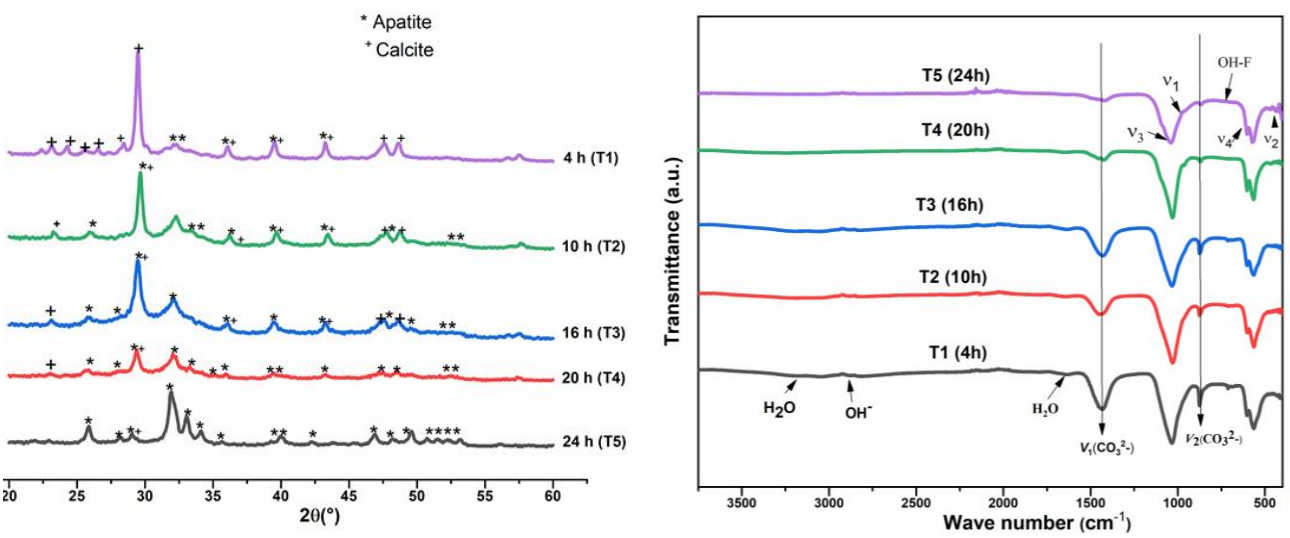

(a) **(b)**

Fig. 8 (a) XRD patterns of synthesized samples as function of grinding duration (Ω = 450 rpm, mp = 1.2 g and Nb = 6) (b) IR spectra of samples prepared at different milling time (a. u. arbitrary units)

Fig. 8 (b) shows the infrared spectra of the prepared samples with different grinding times (T1-T5). The all spectra demonstrated the existence of the same bands observed in the three previous cases as shown in **Fig. 2 (b)**, **Fig. 4 (b)** and **Fig. 6 (b)**. For a grinding time of more than 10 h, Infrared spectra show shoulders observed around 1637 cm-1 corresponding to the vibration modes of the adsorbed water molecules [28]. All spectra show that the fact of increasing the milling time (for 4h to 24h) decreases the intensity of the wide bands attributed to the vibration of water molecules in the region 2500-3700 cm^{-1} [10]. The bands of hydroxide ions characteristic of hydroxyfluorapatite are observed at 3568 cm^{-1} and 631 cm^{-1}. The bands observed around 1420, 1464 and 866 cm^{-1} correspond to the vibration of the CO_3^{2-} groups. These bands are compatible with the presence of type B carbonates [52],[56]. The intensities of the bands attributed to the phosphate groups increase and become more defined as the grinding time increases. In addition, the IR spectra show that the of the carbonate bands intensities decrease while increasing grinding time. This result explains the increase of the apatite content with the increases of milling time and conversely for the calcite content which decreases with

the increase of the milling time. Fahami *et al.* [43] concluded that the chemical composition of initial materials and the milling time are important parameters that affect the structural properties of product *via* mechanochemical process. This result is in accordance with the results of the XRD.

When the grinding duration raises from 4 to 24 h, while the injected shock power remains constant equal to 8.32 W/g, the cumulated energy increases from 33.26 Wh/g to 199.56 Wh/g (**Table 2**). This increase of the cumulated energy induces a proportional increase of the content of the synthesized HFA phase from 25.2% to 99.6% and a proportional decrease of the calcite content from 76.9 to 0.4% (**Table 2**). Specific surface area increases (**Table 2**) as far as the milling duration increases, *i.e.* with the increase of E_{cum}. Hydrodynamic diameter has the inverse tendency than the D_{BET}. It increases as the cumulated energy goes up. Additionally, a high milling duration leads to larger sized aggregates (**Table 2**).

Raman spectra of the hydroxyfluorapatite samples synthesized at 4, 10, 16, 20 and 24 h are characteristic of apatite phase as shown in **Fig. 9 (a)** and **(b)**. All spectra show bands that can be assigned to phosphate groups in an apatite environment [28],[57]. However, the spectrum of the HFA sample synthesized at 4 h clearly shows the most intense vibration bands corresponding to the carbonate groups and the bands attributed to the phosphate group around 960 cm^{-1} have very low intensities [45]. These results may explain the presence of calcium carbonate on the final composition of powder and incomplete reaction of the synthesis of HFA. The stretching bands characteristics of PO_4^{3-} confirm the formation of hexagonal hydroxyfluorapatite. According to [45],[53], the presence of the vibrational bands characteristics of PO_4^{3-} and the hydroxyl group located respectively at 961 cm^{-1} and 603 cm^{-1} confirm the formation of pure hexagonal hydroxyapatite. The intensities of these bands indicate that a significant proportion of the carbonates resulting from the reagents have been incorporated into the apatite phase. Both IR and Raman spectroscopy results confirm the formation of monophasic hydroxyapatite. The intensity of the band of apatite increases in function of milling duration and especially from 10h. **Fig. 9 (b)** clearly shows that the intensity of the calcium carbonate

vibration band around 1110 cm^{-1} decreases with the increase of grinding duration from 4 h to 24 h. Intensity of the apatite vibration bands around 960-962 cm^{-1} increases with the increase of the grinding duration. It can be deduced that the apatite phase content increases with the increase of grinding duration and *vice versa* for calcite. These results do watch those reported by [13],[23]. Indeed, these authors have observed that an increase in the crystallinity of the apatite profile with higher milling times was clearly noticed [23]. It is important, notices that the vibration bands of water and hydroxyl exist in all spectra of samples synthesized at different grinding durations. The Raman results are in agreement with those obtained by XRD and IR techniques.

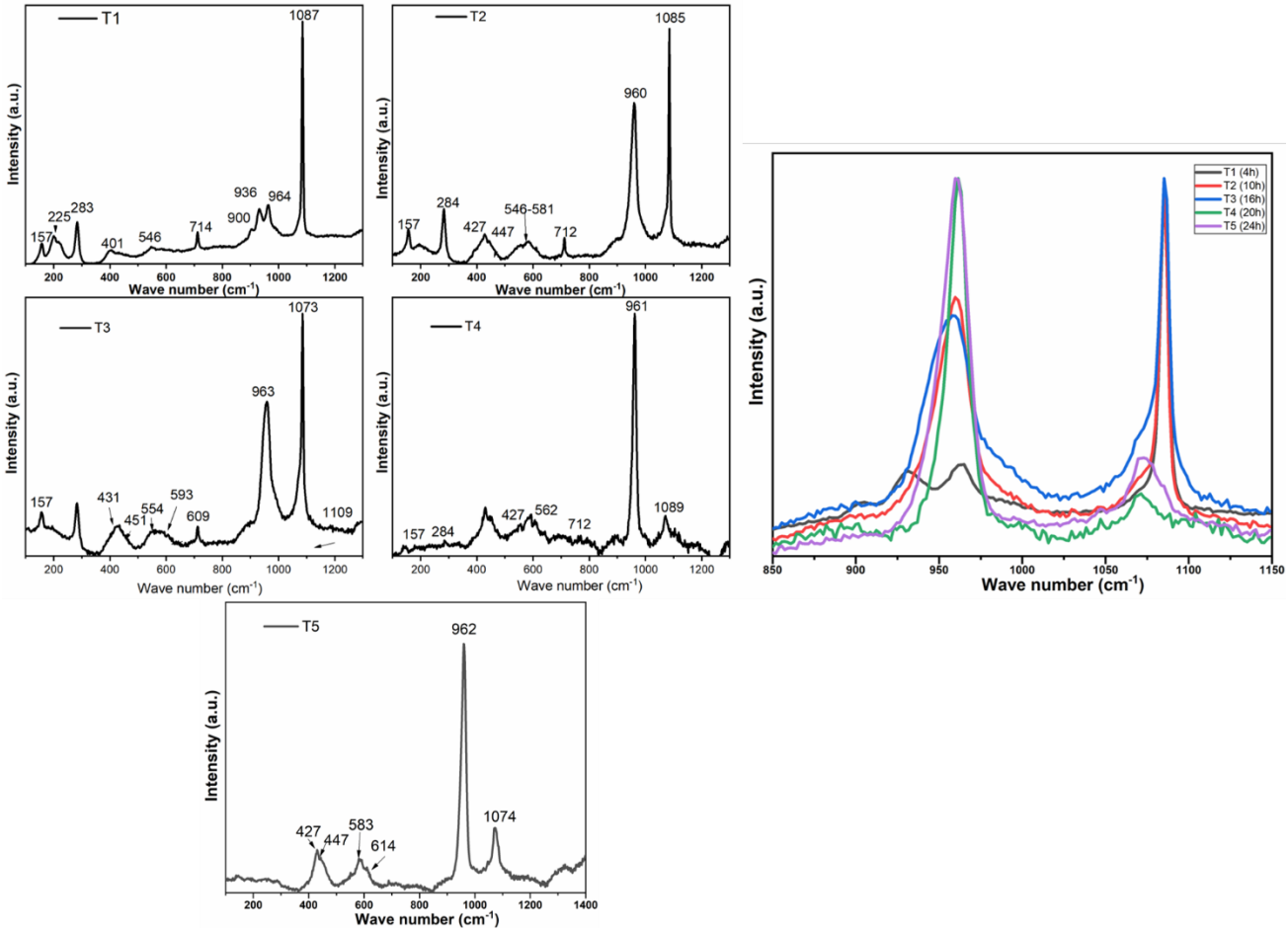

Fig. 9 (a) Raman spectra of samples prepared at different milling durations and (b) Zoom on the PO_4^{3-} (υ4) and calcite (υ1) vibration peaks (a. u. arbitrary units)

Fig. S8 shows the variation of the apatite content, the cumulated energy (E_{cum}) and the surface specific area as a function of the milling duration. This figure shows that at constant injected shock

power, the apatite content increases progressively to reach 35.9% after 16 h of milling and then undergoes a fast increase to reach 99.0% after 24 h of milling. The specific surface area increases when increasing the grinding duration with the same tendency as the apatite content and reach 38.7 m^2/g after 24h of milling.

According to Abdellaoui *et al.*[18],[21], for short grinding times (4 to 16 h), the synthesized material seems showing a resistance for storing the accumulated energy in the form of defects, responsible for the transformation of the starting reagents towards the apatite phase. So, when increasing the milling time, the defect density increases slowly and induces the creation of new specific area (by grain fracture or shear) at a low rate. The apatite content follows the same tendency and increases at a low rate. This suggests that for low milling time, the major fraction of the cumulated energy is transformed to a calorific energy which serves to heat the material, instead of defect density which promotes transformation of the starting reagents towards the apatite phase. For long synthesis times (> 20h), reaction becomes more faster suggesting that the material becomes more able to accumulate energy in the form of defects and that the major fraction of the cumulated energy is transformed in the form of defects [49]. Thus, the content of the apatite phase increases rapidly to reach 99.9% after 24 h of grinding.

4.1.5. Comparison of the effect of the different parameters on the apatite phase formation

The results reported here show that the content of the apatite phase increases when increasing the cumulated kinetic energy by increasing either the injected shock power (increasing W, increasing Nb, decreasing mp) or the milling duration t. The efficiency of mechanosynthesis can be evaluated by the HFA formation rate, expressed in apatite wt.% per Wh/g (reported to the cumulated kinetic energy). So, the milling duration parameter t is the most efficient with a formation rate of 0.45. The second efficient parameter is the initial powder mass mp, with a formation rate of 0.31. The third efficient

parameter is the disc rotation speed W, with a formation rate of 0.22. The last efficient parameter is the ball number Nb, with a formation rate of 0.066. For a constant milling duration, the increase of the cumulate kinetic energy is due to the increase of the injected shock power. In this case, the formation rate can be expressed as apatite wt.% per W/g (reported to the injected shock power).

4. *2. Characterization of HFA sample synthesized with optimized milling parameters*

Based on the results obtained previously, it appears that the most optimal values of the parameters to synthesize hydroxyfluorapatite are a disc rotation speed of 450 rpm, an initial mass of powder of 1.2 g, 6 balls (mb= 4.051g and Φ = 10mm) and a milling duration of 24 h.

4.2.1. Chemical analysis

Table S3 gives the atomic concentration, determined by XPS and EDS analysis of the different chemical elements in the sample synthesized with optimal conditions. The Ca/P atomic ratio of the hydroxyfluorapatite phase, determined by XPS analysis, is equal to1.457 and determined by EDS analysis is equal to 1.454. These two values are very close which proves that the powder surface composition is the same as the bulk one (XPS analyses about 3-4 nm in depth). Nevertheless, both remain lower than the stoichiometric atomic ratio of 1.67 in pure hydroxyfluorapatite phase. This shows that the obtained HFA is calcium deficient (sub-stoichiometric) is probably, as supposed by IR investigation, to the presence of carbonate groups in the phosphate sites in the apatite structure [58],[59]. The presence of iron in the synthesized sample (0.19 % (at.)) is due to the contamination induced by the friction between the vial wall and the balls (**Table S3**).

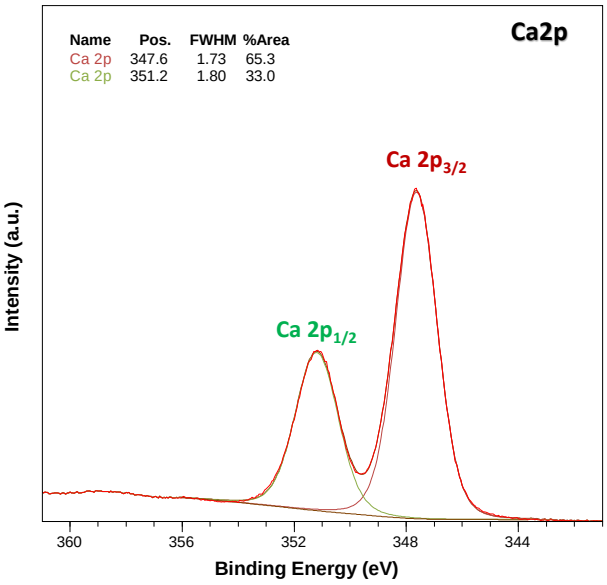
Ca2p
Name Pos. FWHM %Area
Ca 2p 347.6 1.73 65.3
Ca 2p 351.2 1.80 33.0
Ca 2p3/2
Ca 2p1/2
Intensity (a.u.)
360 356 352 348 344
Binding Energy (eV)

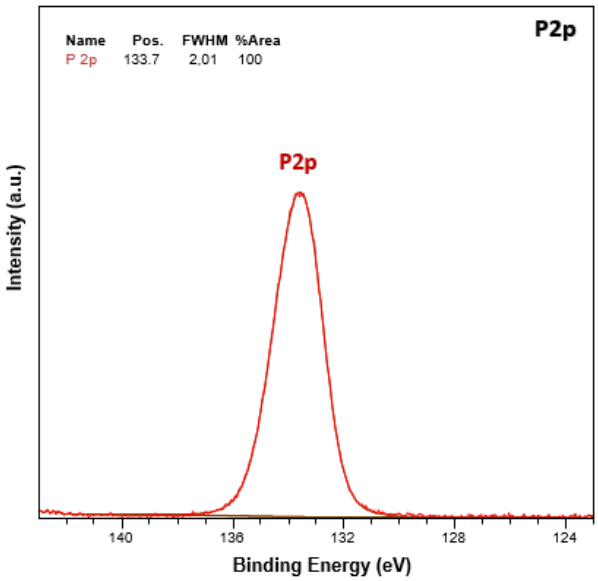
P2p
Name Pos. FWHM %Area
P 2p 133.7 2.01 100
P2p
Intensity (a.u.)
140 136 132 128 124
Binding Energy (eV)

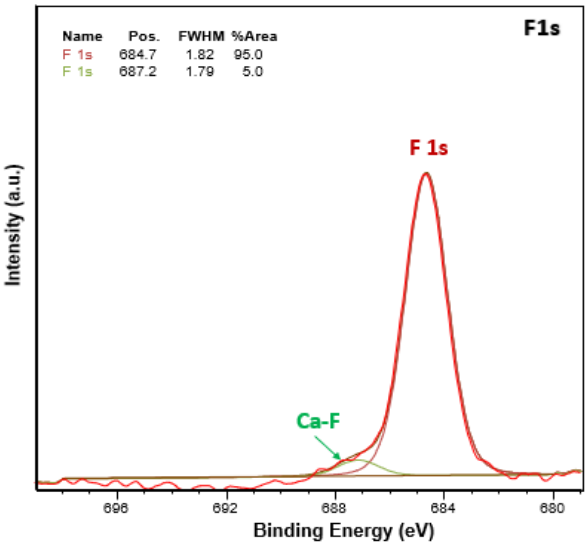
F1s
Name Pos. FWHM %Area
F 1s 684.7 1.82 95.0
F 1s 687.2 1.79 5.0
F 1s
Ca-F
Intensity (a.u.)
696 692 688 684 680
Binding Energy (eV)

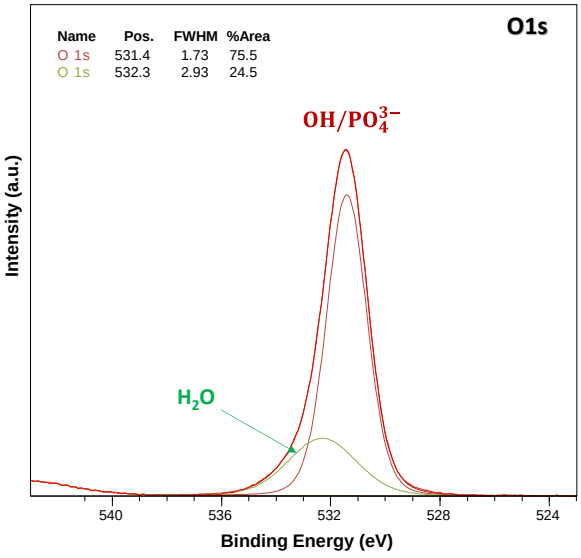
O1s
Name Pos. FWHM %Area
O 1s 531.4 1.73 75.5
O 1s 532.3 2.93 24.5
OH/PO4 3−
H2O
Intensity (a.u.)
540 536 532 528 524
Binding Energy (eV)

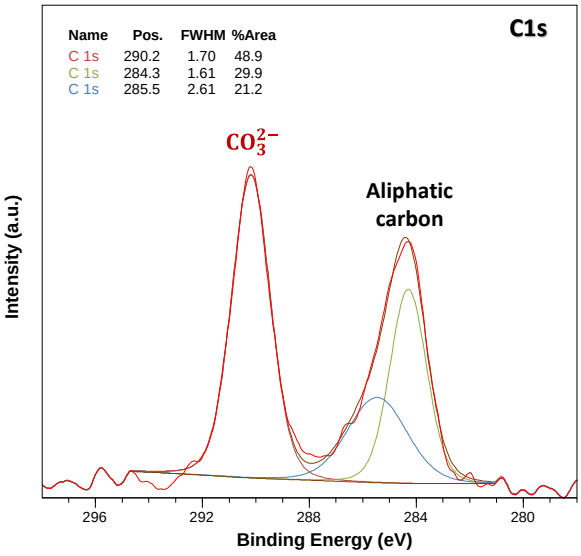
C1s
Name Pos. FWHM %Area
C 1s 290.2 1.70 48.9
C 1s 284.3 1.61 29.9
C 1s 285.5 2.61 21.2
CO3 2−
Aliphatic carbon
Intensity (a.u.)
296 292 288 284 280
Binding Energy (eV)

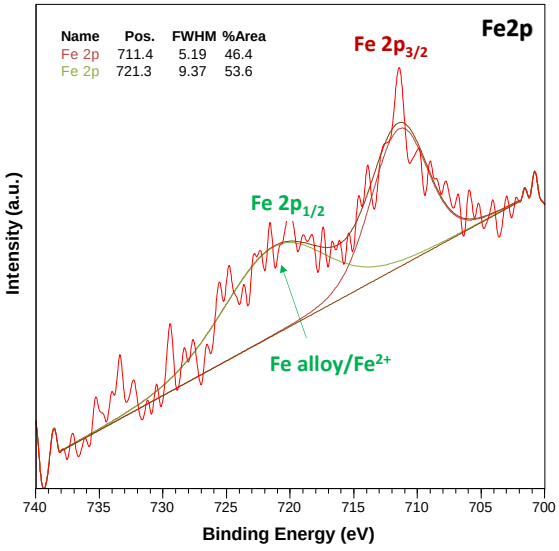
Fe2p
Name Pos. FWHM %Area
Fe 2p 711.4 5.19 46.4
Fe 2p 721.3 9.37 53.6
Fe 2p3/2
Fe 2p1/2
Fe alloy/Fe2+
Intensity (a.u.)
740 735 730 725 720 715 710 705 700
Binding Energy (eV)

Fig. 10 XPS spectra with High-resolution of the hydroxyfluorapatite prepared by mechanosynthesis with the optimal parameters (450 rpm, 1.2g, 6 balls and 24h) (a. u. arbitrary units)

Typical XPS spectra from HFA are shown **Fig. 10**. The Ca2p spectrum is a doublet with Ca $2p_{3/2}$ and $Ca2p_{1/2}$ at 347.6 and 351.2 eV respectively. The P2p peak has its major contribution to 133.1 eV which is typical in apatite. Indeed, all these values are in very good concordance with those observed by Leilei *et al.* [60] (347.2, 350.9 and 133.2eV respectively for Ca $2p_{3/2}$, Ca $2p_{1/2}$ and P2p). The F1s peak is also positioned at the fingerprint fluorine in substituted hydroxyapatite (684.7 eV), as reported by other researchers (684.5 eV in the case of Leilei *et al.*) [51],[61]. The O1 peak is asymmetrical and can be decomposed into two components. The main component located at 531.4 eV may be attributed both to an oxygen bound to a phosphorus atom and corresponds to PO_4^{3-} ions or to the OH^- ions of the apatite structure [58],[62]. The binding energy of the second component at 532.3 eV can be attributed to chemisorbed water (24.5% of the oxygen contribution) [51]. These results clearly match those obtained by Raman and IR analyses which also confirmed the presence of OH, CO_3 and PO_4 groups in the sequence of the apatite structure. The C1s spectrum comprises three peaks: the two located at 284.3 and 285.4 eV can be attributed to aliphatic carbon which exist on the surface due to carbon contamination and the peak at 290.2 eV is characteristic of type B-carbonates as shown by [58]. This component (48.9%) allows to calculate the amount of carbonates at the surface of the powder, which is estimated to 1.8% (**Table S3**). In addition, Fe 2p spectrum is split into Fe 2p1/2 and 2p3/2 due to spin orbit j-j coupling [63]. The Fe 2p3/2 contribution located at 711.4 eV and Fe $2p_{1/2}$ at 721.3 eV may stem from the contamination between the jar wall and the balls leading to the low-percentage of iron oxide and iron alloy as an impurity on the prepared compound (0.2%, **Table S3**).

TGA curve (**Fig. S9**) shows a total mass loss of about 10.6%. Four weight loss stages can be distinguished on the thermogram [23],[64]. The first weight loss, observed between 38-175°C, indicates the evaporation of absorbed water (about 5.4%). The second, of the order of 2.1%, observed between 175 and 295°C, is due to the departure of chemisorbed water molecules (hydroxides). The

third weight loss of about 2.0%, between 295 and 500°C, may be due to the departure of both hydroxides and residual NH_4^+ [64]. The fourth weight loss, of the order of 1%, observed between 500°C and 750°C, is probably due to the departure of the type B carbonate [23]. The TGA results correlate with the XPS and XRD results, since 1.8% (at.) and 0.4% (w) of carbonates are estimated respectively by XPS and XRD. Similarly, 15% (at.) of adsorbed water are observed in XPS (**Fig. 9**).

4.2.2. Morphological study

Fig.11 shows the SEM and TEM analysis of synthesized HFA samples by examining morphology and the particles size. SEM and TEM micrographs clearly show that the sample synthesized by mechanosynthesis is aggregated and consists of nanoparticles (**Fig. 11**). The aggregates can be created by coalescence or welding of particles according to literature [22],[65]. The energy released appears during successive shocks between the balls, wall of jar and powder [56]. TEM observations (**Fig. 11 (c)**) indicate that the aggregates are made up of almost spherical nanocrystals with mean sizes between 10 and 20 nm. These nanocrystals are very well crystallized as proven by High Resolution-TEM observations (**Fig. 11 (d)**).

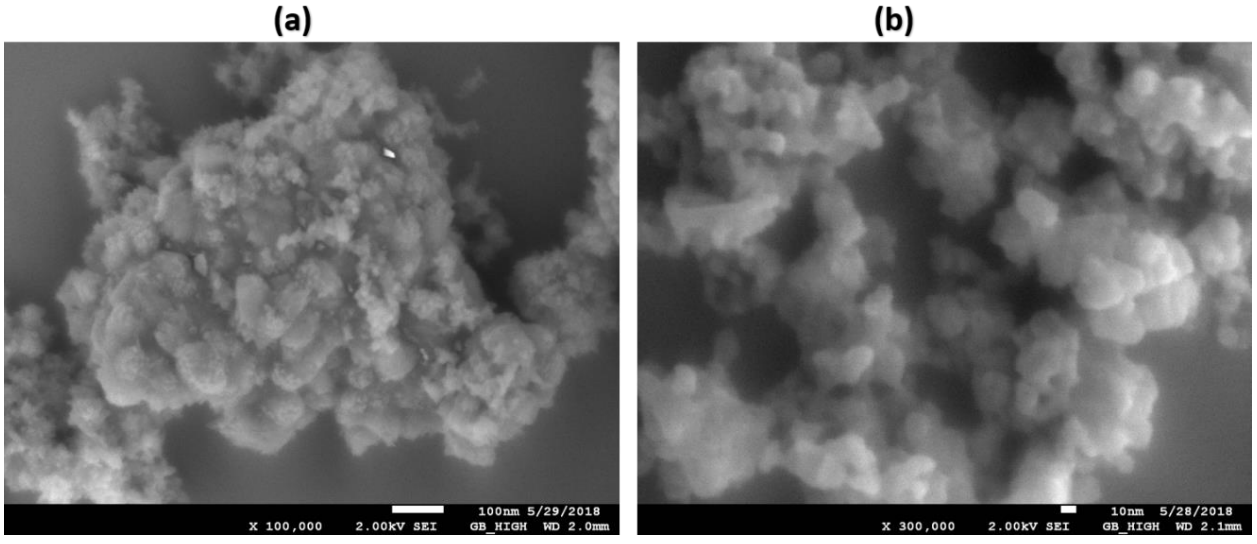

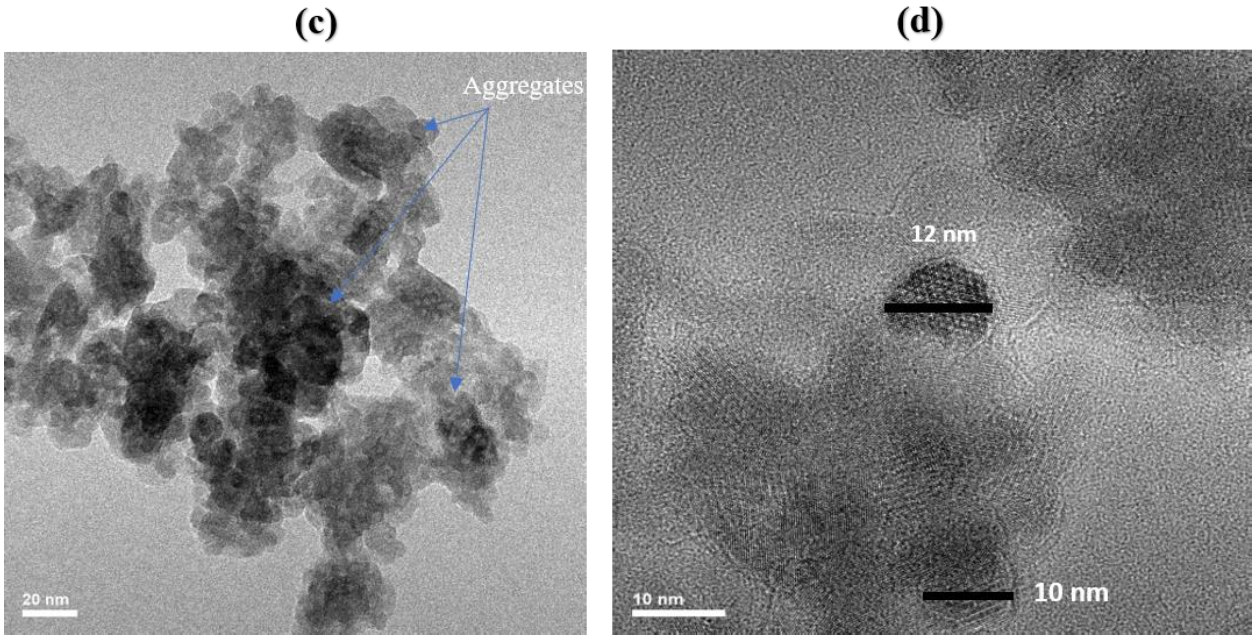

Fig. 11 (**a, b**) SEM images, (**c, d**) TEM and HR-TEM images of the sample synthesized with the optimal milling conditions (450 rpm, 1.2g, 6 balls and 24h)

5. Conclusion

Nanocrystalline hydroxyfluorapatite powders were synthesized by mechanosynthesis *via* a planetary ball mill. The effect of the different milling parameters such as the rotation speed of disc, the grinding duration, the initial powder mass and the number of balls has been carefully studied and optimized to obtain pure nanocrystalline HFA. In this study, the main findings are:

- As the disc rotation speed increases the apatite phase content increases and the calcite phase decreases. It has been deduced that the increase of the disc rotation speed raises the injected shock power and the cumulated kinetic energy.

- The powder initial mass increase leads to a decrease of the injected shock power and of the cumulated kinetic energy at a constant duration. Low initial powder masses tend to accelerate the chemical reaction to obtain the apatite phase.

- Increasing the number of balls increases the injected shock power and the cumulated kinetic energy. With a number of balls equal to 7, there was a decrease in the percentage of the apatite phase. This result may be due to the over filling of the mill so that the mobility of the balls becomes more difficult and therefore the kinetic energy of the balls is reduced.

- The increasing of the grinding duration increases the injected shock power and the cumulated kinetic energy. Structural analyses showed that the desired phase content increases with the grinding duration.

The four studied milling parameters had very important effects on the final content and composition of the desired phase and the experimental results were in agreement with the calculations of the proposed kinematic model. Based on the results obtained, it appeared that the most optimal values of the parameters studied were as follows: 450 rpm, 1.2 g, 6 balls and 24 h of grinding duration.

In addition to XRD, DLS, BET, Raman and IR spectroscopies characterizations of the 16 samples prepared, the optimally prepared sample was examined by a detailed study by XPS elemental analysis, TGA, SEM and TEM. The results obtained by XPS showed that the pure HFA phase was sub-stoichiometric, probably due to the presence of carbonate groups in the HFA structure. Also, this result was confirmed by TGA analysis. Moreover, the positions of the XPS peaks of the different atoms were compatible with the HFA structure. TEM revealed that particles were almost spherical with sizes around 10-20 nm. This optimized powder, prepared by mechanosynthesis, in connection with a model, would be very promising to develop bioceramics and this will be the subject of further studies.

Acknowledgments

Authors would like to thank N. Geoffroy for XRD analysis, Dr. O. Heintz for XPS analysis, Dr. R. Chassagnon for TEM investigations, M. Guerineau for BET analysis, Dr. L. Saviot for Raman analysis, F. Herbst for SEM investigations and Dr. J. Boudon for TGA analysis.

The authors are grateful to King Khalid University for their continuous support during conduction of this work.

Funding Sources

This project was successfully completed with the financial supported received by the “Université de Bourgogne” and the “Conseil Régional Bourgogne Franche-Comté” through the “Plan d'Actions Régional pour l'Innovation (PARI)” and the European Union through the PO FEDER-FSE Bourgogne 2014/2020 programs. This work has been also supported by the EIPHI Graduate School (contract ANR-17-EURE-0002).

References

[1] I. R. Oliveira, T. L. Andrade, K. C. M. L. Araujo, A. P. Luz, V. C. Pandolfelli, « Hydroxyapatite synthesis and the benefits of its blend with calcium aluminate cement », *Ceram. Int.*, vol. 42, n° 2, p. 2542-2549, févr. 2016, doi: 10.1016/j.ceramint.2015.10.056.

[2] I. Nikčević, V. Jokanović, M. Mitrić, Z. Nedić, D. Makovec, D. Uskoković, « Mechanochemical synthesis of nanostructured fluorapatite/fluorhydroxyapatite and carbonated fluorapatite/fluorhydroxyapatite », *J. Solid State Chem.*, vol. 177, n° 7, p. 2565-2574, juill. 2004, doi: 10.1016/j.jssc.2004.03.024.

[3] Y. Yang, H. Zhou, X. Ni, M. Yang, S. Hou, Y. Bi, L. Deng, « Hydroxyapatite: a promising hemostatic component in orthopaedic applications », *Biol. Eng. Med.*, vol. 2, n° 1, 2017, doi: 10.15761/BEM.1000109.

[4] T. T. Roberts, A. J. Rosenbaum, « Bone grafts, bone substitutes and orthobiologics: The bridge between basic science and clinical advancements in fracture healing », *Organogenesis*, vol. 8, n° 4, p. 114-124, oct. 2012, doi: 10.4161/org.23306.

[5] S. Pokhrel, « Hydroxyapatite: Preparation, Properties and Its Biomedical Applications », *Adv. Chem. Eng. Sci.*, vol. 08, n° 04, p. 225-240, 2018, doi: 10.4236/aces.2018.84016.

[6] C. Rey, J. L. Miquel, L. Facchini, A. P. Legrand, M. J. Glimcher, « Hydroxyl groups in bone mineral », *Bone*, vol. 16, n° 5, p. 583-586, mai 1995, doi: 10.1016/8756-3282(95)00101-I.

[7] A. Szcześ, L. Hołysz, E. Chibowski, « Synthesis of hydroxyapatite for biomedical applications », *Adv. Colloid Interface Sci.*, vol. 249, p. 321-330, nov. 2017, doi: 10.1016/j.cis.2017.04.007.

[8] M. A. Zykin, A. V. Vasiliev, L. A. Trusov, R. E. Dinnebier, M. Jansen, P. E. Kazin, « Solid state solubility of copper oxides in hydroxyapatite », *J. Solid State Chem.*, vol. 262, p. 38-43, juin 2018, doi: 10.1016/j.jssc.2018.03.003.

[9] S. Nasr, K. Boughzala, E. Ben Salem, K. Bouzuita, « Characterization of magnesium-substituted fluorapatites prepared by hydrothermal method », *Ann. Chim. Sci. Matér.*, vol. 34, n° 1, p. 1-9, févr. 2009, doi: 10.3166/acsm.34.1-9.

[10] R. H. Ali, H. Ageorges, S. Nasr, E. B. Salem, « Zinc and strontium co-substituted hydroxyfluorapatite: Synthesis, sintering and mechanical properties », *Mater. Res. Bull.*, vol. 112, p. 84-94, avr. 2019, doi: 10.1016/j.materresbull.2018.11.042.

[11] A. Oyane, K. Nakanishi, H. Min Kim, F. Miyaji, T. Kokubo, N. Soga, T. Nakamura, « Sol–gel modification of silicone to induce apatite-forming ability », *Biomaterials*, vol. 20, n° 1, p. 79-84, janv. 1999, doi: 10.1016/S0142-9612(98)00146-X.

[12] N. Millot, S. Begin-Colin, P. Perriat, G. Le Caër, « Structure, Cation Distribution, and Properties of Nanocrystalline Titanomagnetites Obtained by Mechanosynthesis: Comparison with Soft Chemistry », *J. Solid State Chem.*, vol. 139, n° 1, p. 66-78, août 1998, doi: 10.1006/jssc.1998.7808.

[13] C. Mochales, R. M. Wilson, S. E. P. Dowker, M.-P. Ginebra, « Dry mechanosynthesis of nanocrystalline calcium deficient hydroxyapatite: Structural characterisation », *J. Alloys Compd.*, vol. 509, n° 27, p. 7389-7394, juill. 2011, doi: 10.1016/j.jallcom.2011.04.033.

[14] M. Abdellaoui, E. Gaffet, « A mathematical and experimental dynamical phase diagram for ball-milled Ni10Zr7 », *J. Alloys Compd.*, vol. 209, n° 1-2, p. 351-361, juill. 1994, doi: 10.1016/0925-8388(94)91124-X.

[15] L. Pei, T. Tsuzuki, A. Dodd, M. Saunders, « Synthesis of calcium chlorapatite nanoparticles and nanorods via a mechanically-induced solid-state displacement reaction and subsequent heat treatment », *Ceram. Int.*, vol. 43, n° 14, p. 11410-11414, oct. 2017, doi: 10.1016/j.ceramint.2017.05.350.

[16] M. Abdellaoui, C. Djega-Mariadassou, E. Gaffet, « Structural study of Fe□Si nanostructured materials », *J. Alloys Compd.*, vol. 259, n° 1-2, p. 241-248, août 1997, doi: 10.1016/S0925-8388(97)00102-3.

[17] C. C. Koch, J. D. Whittenberger, « Mechanical milling/alloying of intermetallics », *Intermetallics*, vol. 4, n° 5, p. 339-355, janv. 1996, doi: 10.1016/0966-9795(96)00001-5.

[18] M. Abdellaoui, E. Gaffet, « The physics of mechanical alloying in a planetary ball mill: Mathematical treatment », *Acta Metall. Mater.*, vol. 43, n° 3, p. 1087-1098, mars 1995, doi: 10.1016/0956-7151(95)92625-7.

[19] C. Suryanarayana, « Mechanical alloying and milling », *Prog. Mater. Sci.*, p. 184, 2001.

[20] X. Devaux, Ch. Laurent, A. Rousset, « Chemical synthesis of metal nanoparticles dispersed in alumina », *Nanostructured Mater.*, vol. 2, nº 4, p. 339-346, juill. 1993, doi: 10.1016/0965-9773(93)90174-A.

[21] M. Abdellaoui, D. Cracco, A. Percheron-Guegan, « Structural investigation and solid-H2 reaction of Mg2Ni rich nanocomposite materials elaborated by mechanical alloying », *J. Alloys Compd.*, vol. 293-295, p. 501-507, déc. 1999, doi: 10.1016/S0925-8388(99)00475-2.

[22] B. Nasiri-Tabrizi, A. Fahami, R. Ebrahimi-Kahrizsangi, « Effect of milling parameters on the formation of nanocrystalline hydroxyapatite using different raw materials », *Ceram. Int.*, vol. 39, nº 5, p. 5751-5763, juill. 2013, doi: 10.1016/j.ceramint.2012.12.093.

[23] T. Mandal, B. K. Mishra, A. Garg, D. Chaira, « Optimization of milling parameters for the mechanosynthesis of nanocrystalline hydroxyapatite », *Powder Technol.*, vol. 253, p. 650-656, févr. 2014, doi: 10.1016/j.powtec.2013.12.026.

[24] S. Lala, B. Satpati, S. K. Pradhan, « Sintering behavior and growth mechanism of β-TCP in nanocrystalline hydroxyapatite synthesized by mechanical alloying », *Ceram. Int.*, vol. 42, nº 11, p. 13176-13182, août 2016, doi: 10.1016/j.ceramint.2016.05.109.

[25] E. Mohammadi Zahrani, M. H. Fathi, « The effect of high-energy ball milling parameters on the preparation and characterization of fluorapatite nanocrystalline powder », *Ceram. Int.*, vol. 35, nº 6, p. 2311-2323, août 2009, doi: 10.1016/j.ceramint.2009.01.012.

[26] C. Mochales, H. E. Briak-BenAbdeslam, M. P. Ginebra, A. Terol, J. A. Planell, P. Boudeville, « Dry mechanochemical synthesis of hydroxyapatites from DCPD and CaO: influence of instrumental parameters on the reaction kinetics », *Biomaterials*, vol. 25, nº 7-8, p. 1151-1158, mars 2004, doi: 10.1016/j.biomaterials.2003.08.002.

[27] C. C. Silva, A. G. Pinheiro, M. A. R. Miranda, J. C. Góes, A. S. B. Sombra, « Structural properties of hydroxyapatite obtained by mechanosynthesis », *Solid State Sci.*, vol. 5, nº 4, p. 553-558, avr. 2003, doi: 10.1016/S1293-2558(03)00035-9.

[28] H. Hajji, S. Nasr, N. Millot, E. B. Salem, « Study of the effect of milling parameters on mechanosynthesis of hydroxyfluorapatite using the Taguchi method », *Powder Technol.*, vol. 356, p. 566-580, nov. 2019, doi: 10.1016/j.powtec.2019.08.087.

[29] M. H. Fathi, E. M. Zahrani, « Fabrication and characterization of fluoridated hydroxyapatite nanopowders via mechanical alloying », *J. Alloys Compd.*, vol. 475, nº 1-2, p. 408-414, mai 2009, doi: 10.1016/j.jallcom.2008.07.058.

[30] M. Magini, A. Iasonna, F. Padella, « Ball milling: An experimental support to the energy transfer evaluated by the collision model », *Scr. Mater.*, vol. 34, nº 1, p. 13-19, janv. 1996, doi: 10.1016/1359-6462(95)00465-3.

[31] A. Iasonna, M. Magini, « Power measurements during mechanical milling. An experimental way to investigate the energy transfer phenomena », *Acta Mater.*, vol. 44, nº 3, p. 1109-1117, mars 1996, doi: 10.1016/1359-6454(95)00226-X.

[32] M. V. Krishna, G. B. Narasimha, N. Rajesh, A. M. Xavior, « Optimization of Influential Parameters on Mechanical Behaviour of AlMg1 SiCu Hybrid Metal Matrix Composites using Taguchi Integrated Fuzzy Approach », *Mater. Today Proc.*, vol. 2, nº 4-5, p. 1464-1468, 2015, doi: 10.1016/j.matpr.2015.07.071.

[33] M. Abdellaoui, E. Gaffet, « Mechanical alloying in a planetary ball mill : kinematic description », *J. Phys. IV*, vol. 04, nº C3, p. C3-291-C3-296, févr. 1994, doi: 10.1051/jp4:1994340.

[34] M. Kavitha, R. Subramanian, K. S. Vinoth, R. Narayanan, G. Venkatesh, N. Esakkiraja, « Optimization of process parameters for solution combustion synthesis of Strontium substituted Hydroxyapatite nanocrystals using Design of Experiments approach », *Powder Technol.*, vol. 271, p. 167-181, févr. 2015, doi: 10.1016/j.powtec.2014.10.046.

[35] G. A. Martin, « Détermination des tailles de particules métalliques et de leur distribution en catalyse hétérogène », *Rev. Phys. Appliquée*, vol. 16, nº 5, p. 181-191, 1981, doi: 10.1051/rphysap:01981001605018100.

[36] M. Abdellaoui, E. Gaffet, « Mechanical alloying in a planetary ball mill : kinematic description », *J. Phys. IV*, vol. 04, nº C3, p. C3-291-C3-296, févr. 1994, doi: 10.1051/jp4:1994340.

[37] P. P. Chattopadhyay, I. Manna, S. Talapatra, S. K. Pabi, « A mathematical analysis of milling mechanics in a planetary ball mill », *Mater. Chem. Phys.*, vol. 68, nº 1-3, p. 85-94, févr. 2001, doi: 10.1016/S0254-0584(00)00289-3.

[38] N. Gmati, K. Boughzala, M. Abdellaoui, K. Bouzouita, « Mechanochemical synthesis of strontium britholites: Reaction mechanism », *Comptes Rendus Chim.*, vol. 14, nº 10, p. 896-903, oct. 2011, doi: 10.1016/j.crci.2011.04.005.

[39] M. E. Fleet, « Infrared spectra of carbonate apatites: ν2-Region bands », *Biomaterials*, vol. 30, nº 8, p. 1473-1481, mars 2009, doi: 10.1016/j.biomaterials.2008.12.007.

[40] H. Ammar, S. Nasr, H. Ageorges, E. B. Salem, « Sintering and mechanical properties of magnesium containing hydroxyfluorapatite », *J. Aust. Ceram. Soc.*, nov. 2019, doi: 10.1007/s41779-019-00422-7.

[41] M. E. Fleet, X. Liu, « Local structure of channel ions in carbonate apatite », *Biomaterials*, vol. 26, nº 36, p. 7548-7554, déc. 2005, doi: 10.1016/j.biomaterials.2005.05.025.

[42] M. E. Fleet, X. Liu, « Location of type B carbonate ion in type A–B carbonate apatite synthesized at high pressure », *J. Solid State Chem.*, vol. 177, nº 9, p. 3174-3182, sept. 2004, doi: 10.1016/j.jssc.2004.04.002.

[43] A. Fahami, B. Nasiri-Tabrizi, « Mechanochemical behavior of CaCO3–P2O5–CaF2 system to produce carbonated fluorapatite nanopowder », *Ceram. Int.*, vol. 40, nº 9, p. 14939-14946, nov. 2014, doi: 10.1016/j.ceramint.2014.06.091.

[44] A. Antonakos, E. Liarokapis, T. Leventouri, « Micro-Raman and FTIR studies of synthetic and natural apatites », *Biomaterials*, vol. 28, nº 19, p. 3043-3054, juill. 2007, doi: 10.1016/j.biomaterials.2007.02.028.

[45] G. Penel, G. Leroy, C. Rey, E. Bres, « MicroRaman Spectral Study of the PO 4 and CO 3 Vibrational Modes in Synthetic and Biological Apatites », *Calcif. Tissue Int.*, vol. 63, nº 6, p. 475-481, déc. 1998, doi: 10.1007/s002239900561.

[46] A. Gianfagna, S. Mazziotti-Tagliani, A. Croce, M. Allegrina, C. Rinaudo, « As-RICH APATITE FROM MT. CALVARIO: CHARACTERIZATION BY MICRO-RAMAN SPECTROSCOPY », *Can. Mineral.*, vol. 52, nº 5, p. 799-808, oct. 2014, doi: 10.3749/canmin.1400039.

[47] J. Sun, Z. Wu, H. Cheng, Z. Zhang, R. L. Frost, « A Raman spectroscopic comparison of calcite and dolomite », *Spectrochim. Acta. A. Mol. Biomol. Spectrosc.*, vol. 117, p. 158-162, janv. 2014, doi: 10.1016/j.saa.2013.08.014.

[48] M. N. Salimi, R. H. Bridson, L. M. Grover, G. A. Leeke, « Effect of processing conditions on the formation of hydroxyapatite nanoparticles », *Powder Technol.*, vol. 218, p. 109-118, mars 2012, doi: 10.1016/j.powtec.2011.11.049.

[49] I. Sahli, O. Ghodbane, M. Abdellaoui, « Elaboration and electrochemical characterization of LaZr2Cr4Ni5-based metal hydride alloys », *Ionics*, vol. 22, nº 10, p. 1973-1983, oct. 2016, doi: 10.1007/s11581-016-1725-y.

[50] H. Ghayour, M. Abdellahi, M. Bahmanpour, « Optimization of the high energy ball-milling: Modeling and parametric study », *Powder Technol.*, vol. 291, p. 7-13, avr. 2016, doi: 10.1016/j.powtec.2015.12.004.

[51] H. Tanaka, A. Yasukawa, K. Kandori, T. Ishikawa, « Surface structure and properties of fluoridated calcium hydroxyapatite », *Colloids Surf. Physicochem. Eng. Asp.*, vol. 204, nº 1-3, p. 251-259, mai 2002, doi: 10.1016/S0927-7757(02)00005-5.

[52] M. Wang, R. Qian, M. Bao, C. Gu, P. Zhu, « Raman, FT-IR and XRD study of bovine bone mineral and carbonated apatites with different carbonate levels », *Mater. Lett.*, vol. 210, p. 203-206, janv. 2018, doi: 10.1016/j.matlet.2017.09.023.

[53] F. Errassifi, S. Sarda, A. Barroug, A. Legrouri, H. Sfihi, C. Rey, « Infrared, Raman and NMR investigations of risedronate adsorption on nanocrystalline apatites », *J. Colloid Interface Sci.*, vol. 420, p. 101-111, avr. 2014, doi: 10.1016/j.jcis.2014.01.017.

[54] N. Millot, S. Begin-Colin, P. Perriat, G. Le Caër, « Structure, Cation Distribution, and Properties of Nanocrystalline Titanomagnetites Obtained by Mechanosynthesis: Comparison with Soft Chemistry », *J. Solid State Chem.*, vol. 139, n° 1, p. 66-78, août 1998, doi: 10.1006/jssc.1998.7808.

[55] H. Ashrafizadeh, M. Ashrafizaadeh, « Influence of processing parameters on grinding mechanism in planetary mill by employing discrete element method », *Adv. Powder Technol.*, vol. 23, n° 6, p. 708-716, nov. 2012, doi: 10.1016/j.apt.2011.09.002.

[56] A. Fahami, B. Nasiri-Tabrizi, G. W. Beall, B. Pingguan-Murphy, « Effect of ion concentration on mechanosynthesis of carbonated chlorapatite nanopowders », *Mater. Lett.*, vol. 146, p. 16-19, mai 2015, doi: 10.1016/j.matlet.2015.01.149.

[57] B. Nasiri-Tabrizi, P. Honarmandi, R. Ebrahimi-Kahrizsangi, P. Honarmandi, « Synthesis of nanosize single-crystal hydroxyapatite via mechanochemical method », *Mater. Lett.*, vol. 63, n° 5, p. 543-546, févr. 2009, doi: 10.1016/j.matlet.2008.11.030.

[58] D.L. Goloshchapov, M.S. Gushchin, V.M. Kashkarov, P.V. Seredin, Y.A. Ippolitov, N.O. Khmelevsky, A.Yu. Aksenenko « XPS and XANES studies of biomimetic composites based on B-type nano-hydroxyapatite », *Results Phys.*, vol. 9, p. 1386-1387, juin 2018, doi: 10.1016/j.rinp.2018.04.065.

[59] M. Valletregi, « Synthesis and characterisation of calcium deficient apatite », *Solid State Ion.*, vol. 101-103, p. 1279-1285, nov. 1997, doi: 10.1016/S0167-2738(97)00213-0.

[60] Z. Leilei, L. Hejun, L. Kezhi, F. Qiangang, Z. Yulei, L. Shoujie, « Synthesis and characterization of nanobelt-shaped Na, F and carbonate multi-substituted hydroxyapatite », *Mater. Lett.*, vol. 138, p. 48-51, janv. 2015, doi: 10.1016/j.matlet.2014.09.099.

[61] K. Cheng, S. Zhang, W. Weng, « The F content in sol–gel derived FHA coatings: an XPS study », *Surf. Coat. Technol.*, vol. 198, n° 1-3, p. 237-241, août 2005, doi: 10.1016/j.surfcoat.2004.10.023.

[62] S. Kačiulis, G. Mattogno, L. Pandolfi, M. Cavalli, G. Gnappi, A. Montenero, « XPS study of apatite-based coatings prepared by sol–gel technique », *Appl. Surf. Sci.*, vol. 151, n° 1-2, p. 1-5, sept. 1999, doi: 10.1016/S0169-4332(99)00267-6.

[63] G. Thomas, F. Demoisson, R. Chassagnon, E. Popova, N. Millot, « One-step continuous synthesis of functionalized magnetite nanoflowers », *Nanotechnology*, vol. 27, n° 13, p. 135604, avr. 2016, doi: 10.1088/0957-4484/27/13/135604.

[64] K. Tônsuaadu, M. Peld, T. Leskelä, R. Mannonen, L. Niinistö, M. Veiderma, « A thermoanalytical study of synthetic carbonate-containing apatites », *Thermochim. Acta*, vol. 256, n° 1, p. 55-65, mai 1995, doi: 10.1016/0040-6031(94)02169-O.

[65] P. Baláž, *Mechanochemistry in nanoscience and minerals engineering*. Berlin: Springer, 2008.